

THS



This is to certify that the

thesis entitled

Design of a Telemetry System

Between the Piston and the Crank Case
of a Combustion Engine

presented by

Hansgert Hascher

has been accepted towards fulfillment of the requirements for

Master degree in Mechanical
of Science Engineering

Hourd & Selevell

Major professor

Date October / 13 / 1994

O-7639

MSU is an Affirmative Action/Equal Opportunity Institution

LIBRARY Michigan State University

PLACE IN RETURN BOX to remove this checkout from your record.

TO AVOID FINES return on or before date due.

DATE DUE	DATE DUE	DATE DUE
·		

MSU is An Affirmative Action/Equal Opportunity Institution ctelectatedus.pm3-p.1

DESIGN OF A TELEMETRY SYSTEM BETWEEN THE PISTON AND THE CRANK CASE OF A COMBUSTION ENGINE

By

Hansgert Hascher

A THESIS

Submitted to
Michigan State University
in partial fulfillment of the requirements
of the degree of

MASTER OF SCIENCE

Department of Mechanical Engineering

ABSTRACT

DESIGN OF A TELEMETRY SYSTEM BETWEEN THE PISTON AND THE CRANK CASE OF A COMBUSTION ENGINE

By

Hansgert Hascher

For many years, temperature and position measurements made from the piston inside a piston engine have been transmitted by electrical wires from the piston to the crank case. Most of these wires broke after only 10 hours (that is less than 500 miles for a car), due to high piston acceleration of several hundred g.

A more reliable system with a wireless signal transmission will now enable engine researchers to collect data from the piston for a much longer time without disassembling the engine. Such a system will also give researchers a tool to monitor pressures between the cylinder wall and piston rings, allowing them to make necessary design changes to reduce emissions.

The telemetry system built by Michigan State University's Engine Research Laboratory is based on a frequency modulated infrared (IR) optical data transmission between the piston (two IR diodes) and crank case (IR photocell). A semiconductor membrane pressure transducer mounted on top of the piston yields the transmitted signal. A reference quartz pressure transducer is mounted inside

the cylinder head. The single-cylinder engine is motored by an electrical motor, and the telemetry power is supplied by batteries attached to the connecting rod.

The two recorded pressure signals are superimposed over the whole range of possible engine speeds. The offset drift of the telemetry system is negligible, even after a long series of measurements.

ACKNOWLEDGMENTS

I would like to take this opportunity to thank those people with whose help this study was possible. First, my major professor Dr. Harold Schock for his help and motivation over one year of project realization; to Bob Turnbull, for his excellent circuit board layout; to Scott Sober for his assistance and preceding investigations and to Tom Stuecken, who machined the engine parts and built the test stand.

I would also like to thank Dr. Fred Trinker, Dr. Tom Kenny and the Ford Motor Company for their financial support.

TABLE OF CONTENTS

		Page
LIST OF TABLES		vii
LIST OF FIGURES		viii
CHAPTER 1 -	INTRODUCTION	1
	1.1 History	1
	1.2 Problem Statement	2
CHAPTER 2 -	EXPERIMENTAL EQUIPMENT	3
	2.1 Piston Engine	3
	2.2 Pressure Transducer	4
	2.3 Infrared Telemetry	4
	A. Pressure Transducer	6
	B. Pressure Receiver	9
	C. F to V Converter	12
	2.4 Piston Engine Test Stand	14
	2.5 Piston Acceleration	16
CHAPTER 3 -	PRELIMINARY TESTING	17
	3.1 Static Pressurization	17
	3.2 First Engine Starts	18
CHAPTER 4 -	MAIN TESTING	21
	4.1 Changes and Repairs	21
	4.2 Temperature inside the Cylinder	22
	4.3 Test Program	23

		Page
CHAPTER 5 -	RESULTS AND DISCUSSION	25
	5.1 System Performance	25
	5.2 Sensor Calibration	25
	5.3 Signal Representation	26
CHAPTER 6	SUMMARY AND CONCLUSIONS	43
APPENDIX		45
LIST OF REFER	ENCES	50

LIST OF TABLES

		Page
Γable 1:	Piston Engine Dimensions	 3
Γable 2 :	Engine Test Schedule	 24

LIST OF FIGURES

		Page
Figure 1:	Complete engine with flywheel and cylinder head	5
Figure 2:	Piston with connecting rod and built-in telemetry	5
Figure 3	Pressure transducer circuit board	7
Figure 4	Pressure receiver circuit board	11
Figure 5	Frequency to voltage circuit board	13
Figure 6:	Complete engine test stand with speed controller	15
Figure 7:	Crank case / crank shaft assembly	15
Figure 8:	Piston Acceleration versus engine speed	16
Figure 9:	Static pressurization assembly	17
Figure 10:	Graph: Cylinder charged with pressurized air	18
Figure 11:	Graph: Cylinder discharged	18
Figure 12:	Graph: Engine start up to continuous speed	19
Figure 13:	Graph: Engine at 860 rpm	19
Figure 14:	Graph: Engine at 1500 rpm	19
Figure 15:	Piston engine test stand with oscilloscope	20
Figure 16:	Piston with sender board and first power supply wires	22
Figure 17:	Piston with sender board and fortified supply wires	22
Figure 18:	Uncorrected compression cycle at 290 rpm	27
Figure 19:	Uncorrected compression cycle at 345 rpm	27
Figure 20:	Uncorrected compression cycle at 497 rpm	28
Figure 21:	Uncorrected compression cycle at 604 rpm	28
Figure 22:	Uncorrected compression cycle at 598 rpm	29
Figure 23:	Uncorrected compression cycle at 711 rpm	29

Figure 24:	Uncorrected compression cycle at 801 rpm	30
Figure 25:	Uncorrected compression cycle at 899 rpm	30
Figure 26:	Uncorrected compression cycle at 1007 rpm	31
Figure 27:	Uncorrected compression cycle at 1099 rpm	32
Figure 28:	Uncorrected compression cycle at 1204 rpm	33
Figure 29:	Corrected compression cycle at 1204 rpm	33
Figure 30:	Uncorrected compression cycle at 1301 rpm	34
Figure 31:	Corrected compression cycle at 1301 rpm	34
Figure 32:	Uncorrected compression cycle at 1400 rpm	35
Figure 33:	Corrected compression cycle at 1400 rpm	35
Figure 34:	Uncorrected compression cycle at 1501 rpm	36
Figure 35:	Corrected compression cycle at 1501 rpm	36
Figure 36:	Uncorrected compression cycle at 1595 rpm	37
Figure 37:	Corrected compression cycle at 1595 rpm	37
Figure 38:	Uncorrected compression cycle at 1700 rpm	38
Figure 39:	Corrected compression cycle at 1700 rpm	38
Figure 40:	Uncorrected compression cycle at 1800 rpm	39
Figure 41:	Corrected compression cycle at 1800 rpm	39
Figure 42:	Uncorrected compression cycle at 1894 rpm	40
Figure 43:	Corrected compression cycle at 1894 rpm	40
Figure 44:	Corrected compression cycle at 2008 rpm	41
Figure 45:	Uncorrected compression cycle at 2095 rpm	42
Figure 46: Figure 47:	Uncorrected compression cycle at 2250 rpm Piston Displacement x	42 45

1.0 INTRODUCTION

1.1 History

Transmitting data from moving parts has always been a challenge in engineering. While most of the solutions are designed for rotating devices, like slip rings and radio frequency telemetries for revolving shafts, telemetry systems for oscillating devices are rare. One reason may be the naturally high acceleration at the turning points of the reciprocating motion. This high acceleration causes all mechanical data links (e.g. wires) to fail after a relatively short time period. Even when these wires are attached (e.g. by glue) to a special "grasshopper" linkage, their life expectancy seldom exceeds 10 hours. To transmit signals from the piston of a combustion engine (e.g. ring displacements, pressures and temperatures) researchers preferred to use this method, tolerating the short test time period. The importance of this engine part for the entire combustion process and the lack of other investigation options justified this costly effort [1, 2]. In the last years IR telemetry devices for slow signals, such as temperatures, have been developed [3]. The advance in electronics now allows the use of these methods in a small, economical system.

1.2 Problem Statement

The objective of this study is to determine the feasibility of a telemetry system without hard-wired contacts between a piston and its crankcase and its demonstration in a motored piston engine. The telemetry system will include an infrared sender mounted within the piston and a receiver unit in the crank case. The motored engine has to operate in a range of 300 to 3500 rpm while data is continuously transmitted. The output signal of the system has to satisfy the usual data recording input requirements (0 to 5 volts). The signal will correspond with the pressure inside the cylinder. The system transducer was mounted on top of the piston, and another transducer mounted within the cylinder head will yield a reference pressure signal.

2.0 EXPERIMENTAL EQUIPMENT

2.1 Piston Engine

The engine used on this test stand is a single cylinder piston engine stripped of all inlet and outlet port gear. An aluminum cylinder head was constructed which only housed the reference transducer and a check valve which allowed air only to enter the cylinder. The motored engine yields a cylinder pressure of approximately 140 psi (about 10 bar) (Figures 1 and 2).

Table 1: Piston Engine Dimensions

Piston Diameter	3.5 "	89 mm
Piston Height	2.75 "	70 mm
Connecting Rod Length	4.375 "	112 mm
Stroke	2.75 "	70 mm
Crank Throw Radius	1.375 "	35 mm
$\lambda = r/1$	0.313	
Compression Ratio	10:1	

2.2 Pressure Transducers

The pressure transducer mounted on top of the piston is one of the smallest sensors available, the KULITE XCQ 093. This transducer has a diameter less than 0.1" and operates up to 250°F (120°C) and 500 psi (35 bar). It has a silicon diaphragm behind a screen into which a Wheatstone bridge is diffused.

For further investigations on firing engines KULITE offers a transducer in the same size that will operate up to 450°F (235°C) and 1500 psi (105 bar).

A KISTLER quartz transducer 6121A2 was used as a reference quartz. Like all quartz based sensors, it has a strong zero drift and needs to be reset before every measurement.

2.3 Infrared Telemetry

The sender of the infrared (IR) telemetry depends essentially on the voltage-to-frequency conversion of the incoming pressure signal. This electrical process can now be realized with one single integrated circuit device, the AD537 (from Analog Device Inc.). With this the sender unit circuit board could be reduced to one square inch, which fits exactly into the piston. A sender unit board in the future will only use one fourth of this area, because of the very compact surface mount technology. The sender circuit board was potted into the piston with silicon rubber compound RTV615 from General Electric Co.

The receiver unit is attached to the crank case housing, supplied by ± 12 DC volts, 5 DC volts and the input signal from the IR-photocell. This photocell sits in the crank case at the same height as the crankshaft bearing.



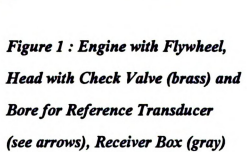




Figure 2: Piston with Rod: Telemetry Board with IR-Diodes within the Piston and Batteries on the ConnectingRod (see arrows)

A. Pressure Transducer Circuit Board

A more detailed description of the circuit is given below and is shown in Figure 3. The sender unit, or pressure transducer circuit board, is powered by four DC 1.5V AAAbatteries. In Figure 3 the sensor symbol symbolizes the Wheatstone bridge of the Kulite pressure transducer. The bridge is diffused into a silicon diaphragm. With that its resistors are subject to the usual semi-conductor temperature sensitivity loss.

The sensor output is connected to an instrumentation amplifier. This circuit is commonly used to measure low voltage signals, where both wires have no ground contact. These signals require a very high impedance input ("differential input", DI), even to the "ground" level. OP-Amps with their very high input impedance between 1 $M\Omega$ and 10 $M\Omega$ are the ideal amplifier for this. Their gain is defined by

The output signal is then voltage-to-frequency converted. A capacitor eliminates high frequency noise on the input signal. Another Capacitor tunes the output frequency range of the two light emitting infrared diodes (IR-LEDs). With a lowpass the power supply is protected from the modulated output frequency of the two IR-LEDs.

The power consumption of this whole circuit is less than 20 mA! In this configuration the pressure transducer circuit would emit a zero Hz frequency at almost zero (ambient) pressure. To raise the "zero" frequency at ambient pressure above 10 kHz the two resistors generate a slight DC offset.

Two IR-diodes guarantee a better signal transmission than a single LED. The second diode replaces a resistor and consumes no additional power. The diodes are mounted at the piston skirt and point along the cylinder liner. There is no "eye contact" at any crank shaft position between the diodes and the receiver photocell, so the data transmission relies only on reflection. Even though the crank case of the piston engine was painted black the signal transmission worked flawlessly.

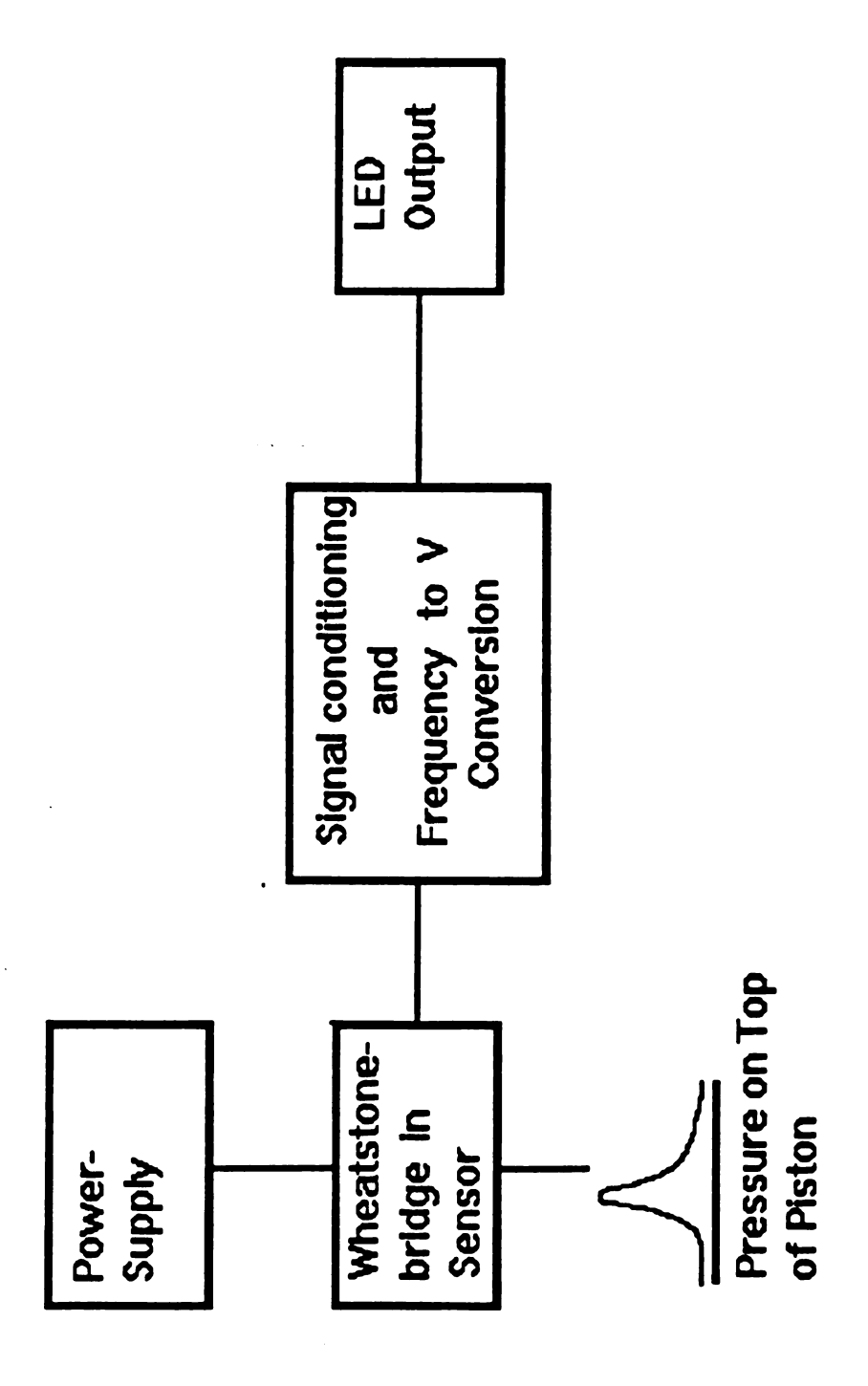


Figure 3: Pressure Transducer
Circuit Board

B. Pressure Receiver Board

The pressure receiver shown in Figure 4 is the signal conditioning unit, usually called "FM receiver", for the receiver IR-photodiode, mounted in the crankcase. It accepts any voltage signal from the diode, regardless of the actual polarity of the diode and delivers a rectangular signal to the F-to-V converter (Figure 5).

To allow easy changes of the receiver photodiodes the circuit was designed to allow both polarities of a diode. After a diode has been installed in a crank case there is no polarity check necessary anymore. It can be connected to the circuit right away and its signal will be recognized.

A photodiode in general can be used as a passive, light-sensitive resistor or as a voltage emitting photocell. In this circuit the photodiode is used as a voltage emitting, active element. The rectangular waveform signal received from the photodiode enters the circuit and is amplified with a special OP-AMP circuit. This guarantees the fastest signal increase, and yields the most rectangular waveform possible.

A special feature of this circuit is the recognition of ambient light. Although this telemetry was designed to operate in an absolute dark crankcase the MSU telemetry system works with ambient light on the photodiode. Any ambient light creates an input offset, which can disable the amplifier to recognize the important signal. For this reason an offset correction is provided.

Several OP-AMPs sum up the total gain of this circuit to 150dB for a 10 kHz signal. For higher frequencies the gain is only slightly reduced. The signal is filtered again before it leaves the unit. At the output of this circuit a rectangular waveform signal with an amplitude of ±0.6 volts enters the following F-to-V converter unit.

The operability of the mounted telemetry system and the big safety margin of this data transmission was demonstrated in a simple test. The engine was opened and the piston, including the sender unit removed from the engine. Even in the regular ambient light of the laboratory the piston could be held up to 4 meters away from the engine to receive a flawless signal.

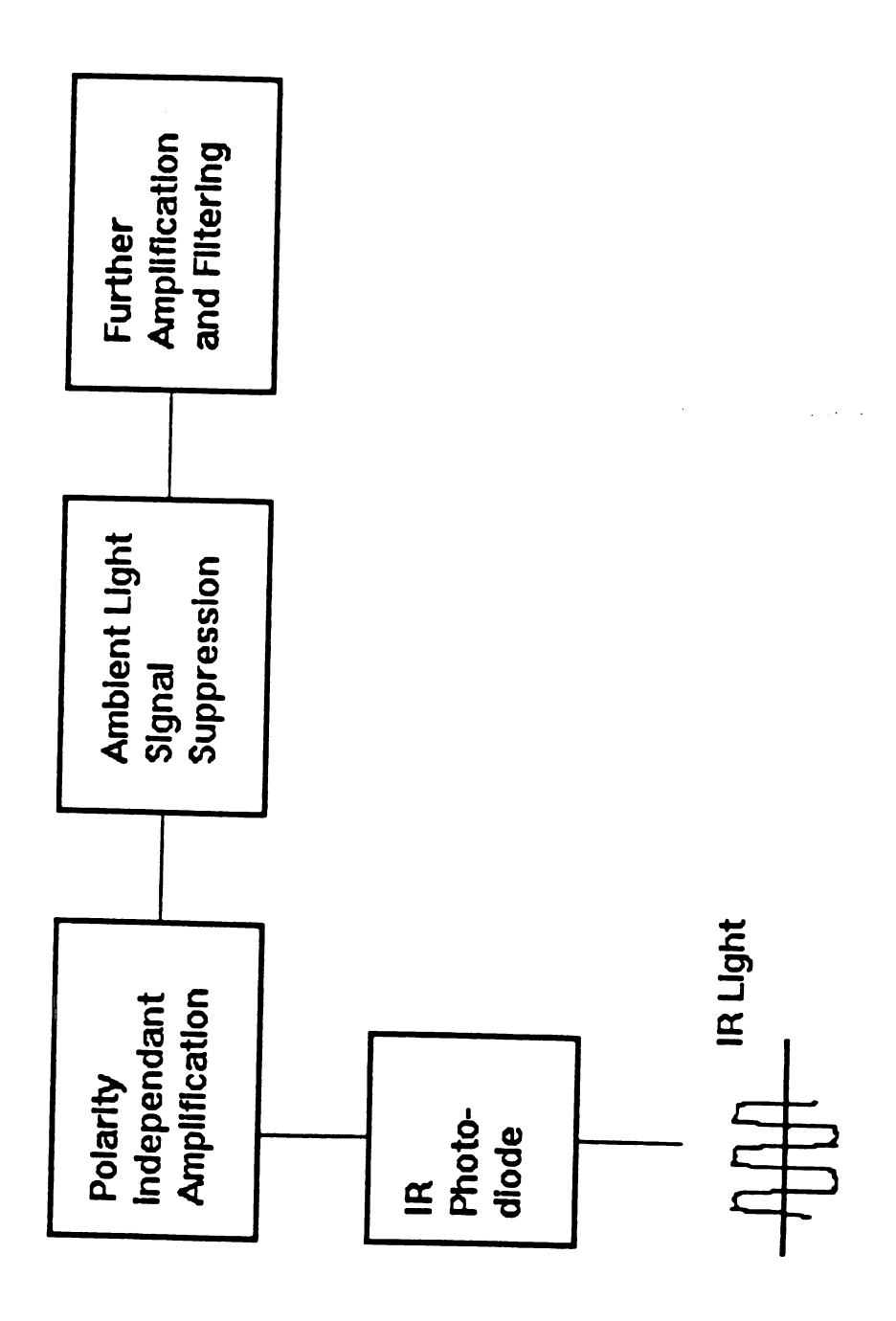


Figure 4: Pressure Receiver
Circuit Board

C. Frequency to Voltage Converter

The frequency to voltage unit converts the incoming ±0.6 volts signal to a TTL level (0 to 5 volts) and transforms the further conditioned signal finally to a smooth analog output signal.

Several OP-AMPs change the incoming signal to a TTL signal. For higher accuracy some multivibrators are used.

The pulse width of the signal can then be calculated to

$$T = R \cdot C = 1.1 \mu sec$$

The pulse width of the signal is finally adjusted with an electronic device that yields a very stable pulse length.

Some consecutive active multiple-order lowpass filters transform the signal to the final analog pressure between 0 and 5 volts. Prerequisites for the filters were a linear phase and no overshoots in the response from the rectangular waveform input signal.

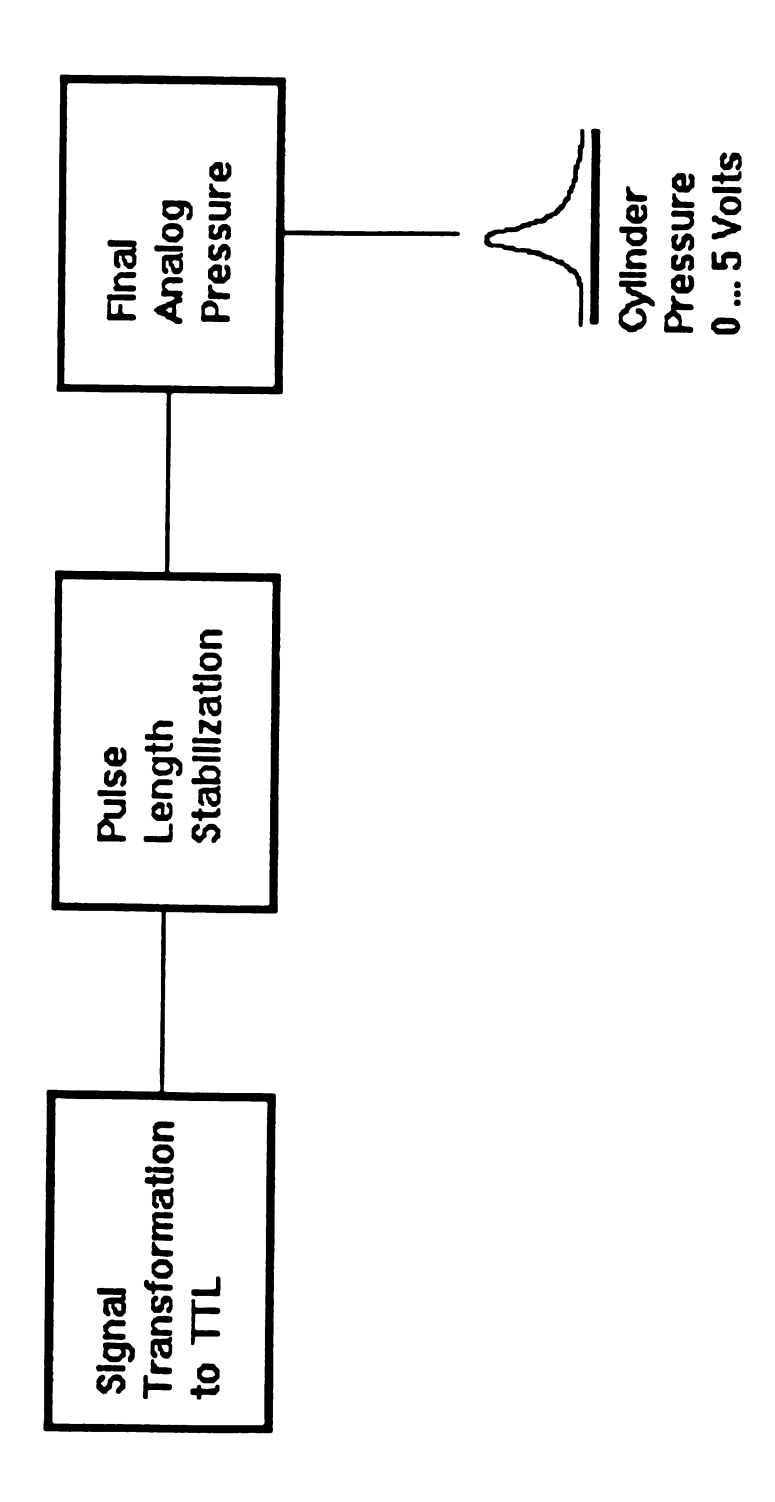


Figure 5: Frequency to Voltage Converter

Circuit Board

2.4 Piston Engine Test Stand

The single-cylinder piston engine was connected to a Louis Allis "Ajusto Speed" 10 HP electrical motor by a Falk 1030T30 coupling (Figure 6). The maximum speed of the motor is 3500 rpm. However, the maximum speed of this test stand never exceeded 2250 rpm because of the noise of the single-cylinder engine, which is only balanced for the first order.

After several test runs, an insulated screw was attached to the connecting rod to allow switching off the telemetry without dismounting and opening the whole engine (Figure 7). This screw can be reached at a certain crankshaft position through an access hole in the crankcase with a long Allen wrench.

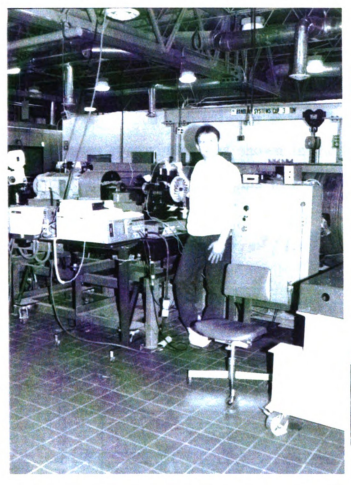




Figure 6: Engine Test Stand with Speed Controller Cabinet (right) and Nicolet 440 Digital Data Storage System

Figure 7: Crank Case / Crank Shaft Assembly with Allen Screw in Connecting Rod to Shortcut Telemetry Power Supply (see arrow)

2.5 Piston Acceleration

The piston acceleration plays a key role in the design of a long lasting circuit board within a piston. Former studies [4] indicated high acceleration on the piston and any parts mounted within.

The piston acceleration is the second derivative of the piston displacement, usually simplified with a Taylor series. The derivation of the exact solution and the series approximation is shown in the appendix. From there the maximum reciprocating acceleration at top dead center (TDC) is taken and plotted below (Figure 8).

$$a_{max}$$
, $TDC = r\omega^2 [1 + \lambda]$

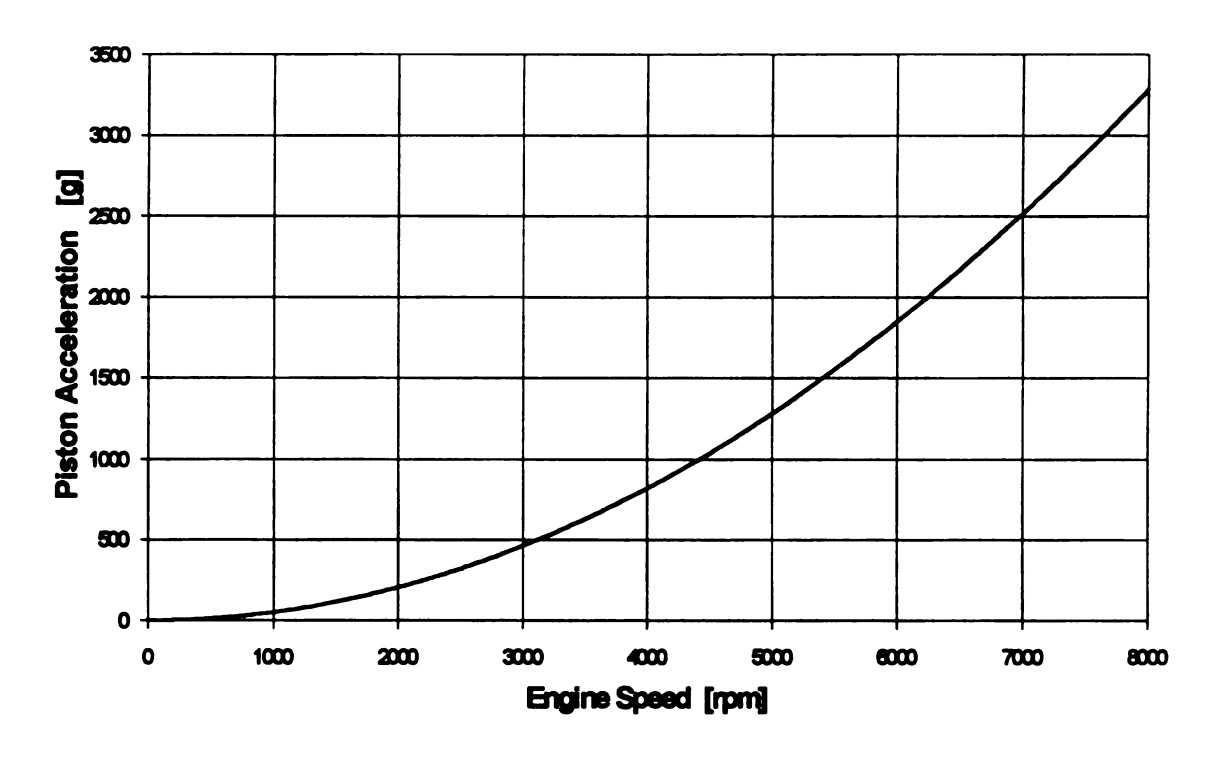


Figure 8: Piston Acceleration of the Telemetry Research Engine

3.0 PRELIMINARY TESTING

3.1 Static Pressurization

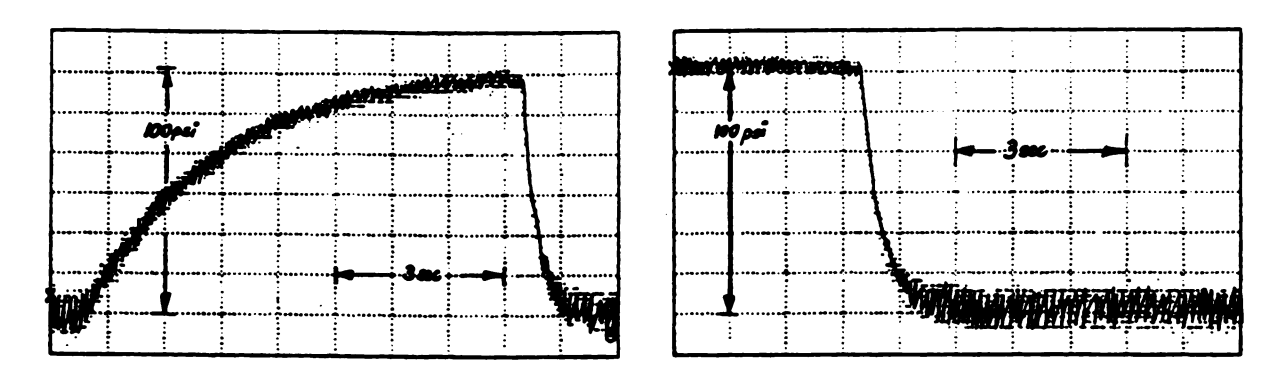
The general function of the telemetry system had to be checked before the engine test stand was put together. The assembled engine was rotated to bottom-dead-center position with running telemetry. A Speedaire 0.75HP compressor delivered pressurized air into a 125 psi, 6 gallon air tank, which was connected to the bore of the suction valve in the cylinder head (Figure 9).



Figure 9: Static Pressurization Assembly with Engine at BDC, Speedaire 6 Gallon Air Tank and Compressor (see arrows) Left: HP54200A Digitizing Oscilloscope with Line Printer

The telemetry responded with an expected signal: caused by the frequency modulation, the transmitted pressure signal has a relatively large noise signal at ambient pressure (which corresponds to a low modulation frequency). As the cylinder pressure rises the modulated frequency rises and with that the signal-noise ratio increases. This effect can be seen in Figure 11 below; the noise is lower at higher pressure before the cylinder is discharged.

However, this test assembly was used only to show the general function of the telemetry.



Cylinder Pressure, Air Pressure Yielded by Compressor System

Figure 10: Cylinder Charged with Compressed Air within 8 Sec

Figure 11: Cylinder Discharged within One Second

3.2 First Engine Starts

After the piston engine test stand was assembled for the first time, several low speed runs were made to check the function of the telemetry. At this time only the voltage was recorded and no actual calibration was taken. However, the results matched satisfactorily with already existing former calibrations (see Figure 13).

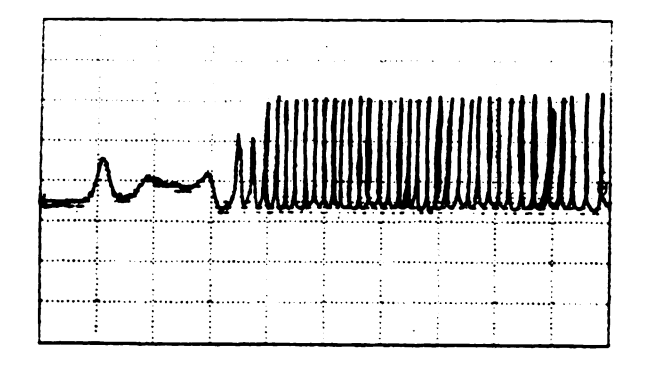


Figure 12: Engine Start, Continuous

Speed Reached after Appr. 3.5 Sec

(Only Telemetry Signal Shown)

Figure 13: Engine at 860 rpm

Graph 1: Telemetry-System

Graph 2: KISTLER Reference

Quartz

After initial measurements, a final recording at 1500 rpm was made (Figure 14). After that the engine was disassembled.

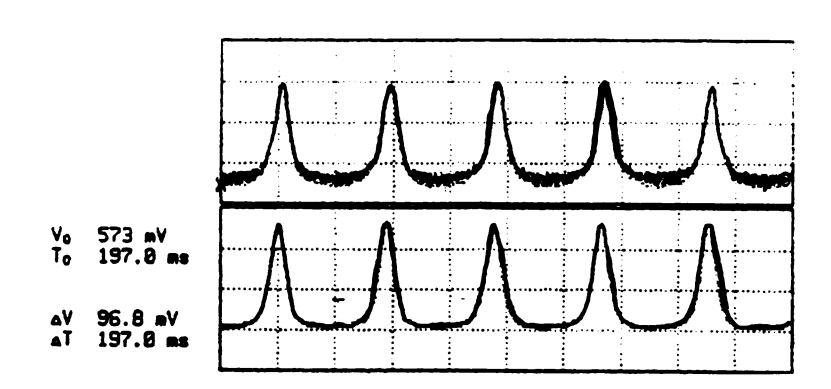


Figure 14: Engine at 1500 rpm

Graph 1: Telemetry-System

Graph 2: KISTLER Reference Quartz

All of these measurements were recorded with a HP54200A Digitizing Oscilloscope and printed with a HP ThinkJet printer (Figure 15).

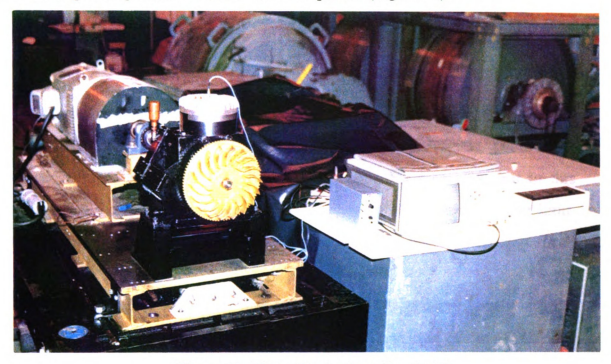


Figure 15: Piston Engine Test Stand with

HP54200A Digitizing Oscilloscope and HP ThinkJet

4.0 Main Testing

4.1 Changes and Repairs

Two problems occurred during the preliminary testing. First, the controller of the 10HP electrical motor did not keep the engine speed stable. Other more balanced engines have achieved a stable speed with this controller, but in this configuration the speed never came to an equilibrium. It increased without limit. This problem was solved with a different controller with less than ± 1 rpm speed deviation.

Second, the wires which connected the batteries (connecting rod) with the sender unit (piston) showed fatigue very soon. In the final runs of the preliminary testing some intermittent signals occured, caused by partly broken power supply wires. This problem could have been resolved with either a continuous power supply by a "grasshopper" linkage made of aluminum bars or a battery power supply with the batteries mounted within the piston. Neither solution was cost-effective for this prototype system. In this project the power supply wires were changed to a fortified cable with a twisted pair of silver- and Teflon-shielded wires (Figure 17). But even this new part showed slight damage at the wire housing after the completion of the main test run (Figure 17, arrow).



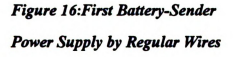




Figure 17:Teflon- and Silver shielded Power Supply Cable with Wear after Main Test Run

This damage is due to the high acceleration of more than 200 g at speeds higher than 2000 rpm (Figure 8).

4.2 Temperature Inside the Cylinder

Due to the temperature sensitivity drift of the Kulite pressure transducer, the temperature inside the cylinder and on top of the piston became important during the test run. In this project only the latter mentioned two pressure signals were measured to prove the feasability of the developed telemetry. Temperature measurments were for efficiency reasons not considered for this prototype.

The temperature inside the cylinder could be evaluated with the equation for isentropic compression [7, 13]:

$$\frac{T_2}{T_1} = \left(\frac{p_2}{p_1}\right)^{\frac{n-1}{n}} = \left(\frac{V_1}{V_2}\right)^{n-1}$$

with 140 psi final pressure and $\kappa = Cp/Cv = 1.4 = n$ (isentropic exponent)

$$T_2 = 1.93 \cdot T_1 = 293$$
°C

The temperature of the cylinder parts must have been significantly below that, because the temperatures on the outside of the cylinder and the oilpan were about 60°C to 70°C. Considering the temperature limitation of the Kulite transducer (250°F, 120°C) and publications about temperatures at oilcooled pistons and at cylinder walls close to the inlet valve [9] the temperature of the Kulite transducer was taken as 100°C.

4.3 Test Program

The test program was scheduled from the lowest constant speed to the highest speed which the engine or the telemetry could stand. For this program we used the digital storage oscilloscope NICOLET 440 with a HP ColorPro pen plotter. All waveforms were stored on a 3.5" floppy disk. Every measured point generates two files, one for every channel, named WAVE_0001.FMT WAVE_0044.FMT.

Table 2: Engine Test Schedule

				Γ
No.	Speed in	Telemetry	KISTLER	Remarks
	rpm	Datafile	Datafile	
1	290	_0001	_0002	
2	345	_0003	_0004	
3	497	_0005	_0006	
4	604	_0007	_0008	no data in last 50% of file
5	598	_0009	_0010	
6	711	_0011	_0012	no data in last 80% of file
7	801	_0013	_0014	
8	899	0015	_0016	no data in last 50% of file
9	1007	_0017	_0018	Motor-Engine System Resonance !
10	1094	_0019	_0020	# bad data stored # (see No.11)
11	1099	_0021	_0022	Motor-Engine System Resonance !
12	1204	_0023	0024	
13	1301	_0025	_0026	
14	1400	_0027	_0028	
15	1501	_0029	_0030	
16	1595	0031	_0032	
17	1700	_0033	_0034	
18	1800	_0035	_0036	
19	1894	_0037	_0038	# partly bad telemetry data #
20	2008	_0039	_0040	Motor-Engine System Resonance !
21	2095	_0041	0041	# bad telemetry data # !
22	2250	_0043	_0044	# bad telemetry data #

5.0 RESULTS AND DISCUSSION

5.1 System Performance

The purpose of this prototype was to show the feasibility of the advanced telemetry. None of the core parts of the telemetry (sender, receiver) or mountings were damaged during testing. The only problems were caused by the power supply wires (see chapter 4.1) and the speed limitations caused by the unbalanced engine.

5.1 Sensor Calibration

The test system was calibrated with the latter mentioned static pressurization assembly (Figure 9). For that the crankshaft was rotated to bottom-dead-center position and pressures of 0, 25, 50, 75 and 100 psi were attached to the cylinder. The voltage output was recorded and the resulting curves of either transducer were linear.

$$Pressure_{Kulite} = (Voltage_{after\ Telemetry} - 0.54) \times 110.6$$
 in psi

$$Pressure_{Kistler} = (Voltage_{Charge\ Amplifier} - 1.2) \times 19.7$$
 in psi

The offset for the Kistler quartz was unstable between each measured point, even with a reset of the charge amplifier before each data acquisition. The offset varied between 1.21 and 1.26 volts, that is 10 psi variation.

5.3 Signal Representation

The quality of the signal transmission can be found by comparing the measured signals against each other. The two signals were sampled into the Nicolet 440 digital storage oscilloscope and displayed and checked and finally stored on a 3.5" floppy disk. After the test run was completed the data was transfered into a PC, scaled in engineering units and plotted with EXCEL 4.0. All Scaling and correction of the temperature sensitivity loss (Kulite sensor) was calculated from the sampled data points in volts. The advanced features of EXCEL 4.0 allowed also a very convenient offset correction for the Kistler quartz signal. The offset could be seen on the chart and in the displayed original data.

The good performance of the telemetry can be seen in the next plots. The KISTLER quartz transducer is known as a very reliable and accurate pressure sensor but needed offset correction for nearly every measured point. This was compensated in EXCEL 4.0. The KULITE sensor signal was never corrected in offset and was adjusted only once for its temperature sensitivity loss after completing the test run (measured point No. 12 and above).

The test run was started at low speed with a cold engine.

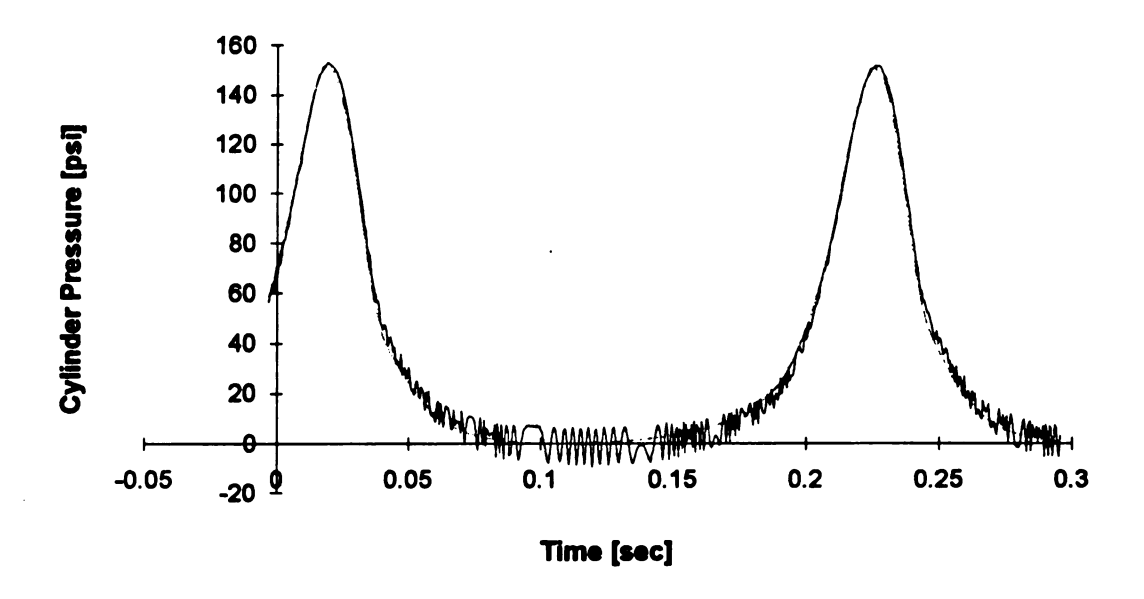


Figure 18: Compression Cycle at 290 rpm
with —— TELEMETRY ---- KISTLER

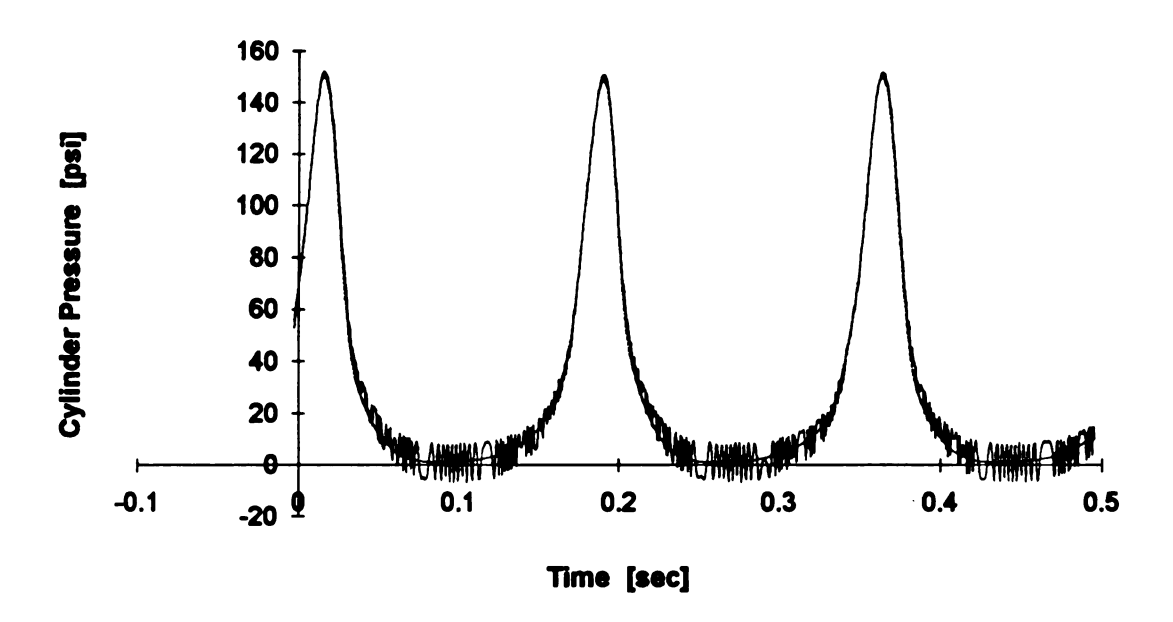


Figure 19: Compression Cycle at 345 rpm
with —— TELEMETRY ---- KISTLER

Both signals are superimposed at higher pressure. At low pressure the frequency modulation shows its characteristic "low-voltage noise" while the KISTLER transducer signal can still be recognized as a smooth curve.

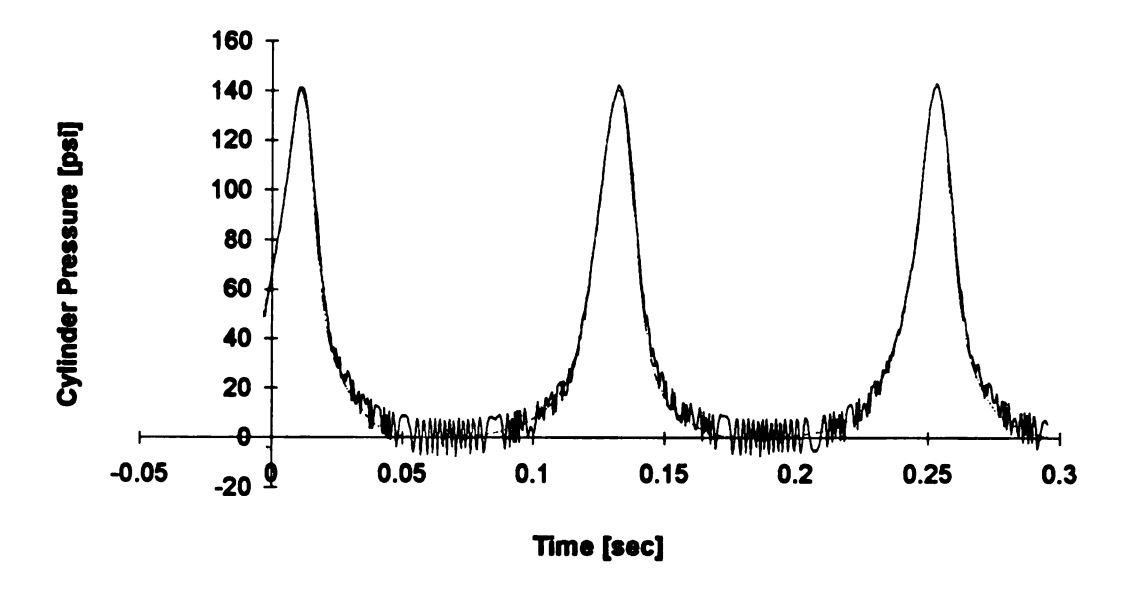


Figure 20: Compression Cycle at 497 rpm

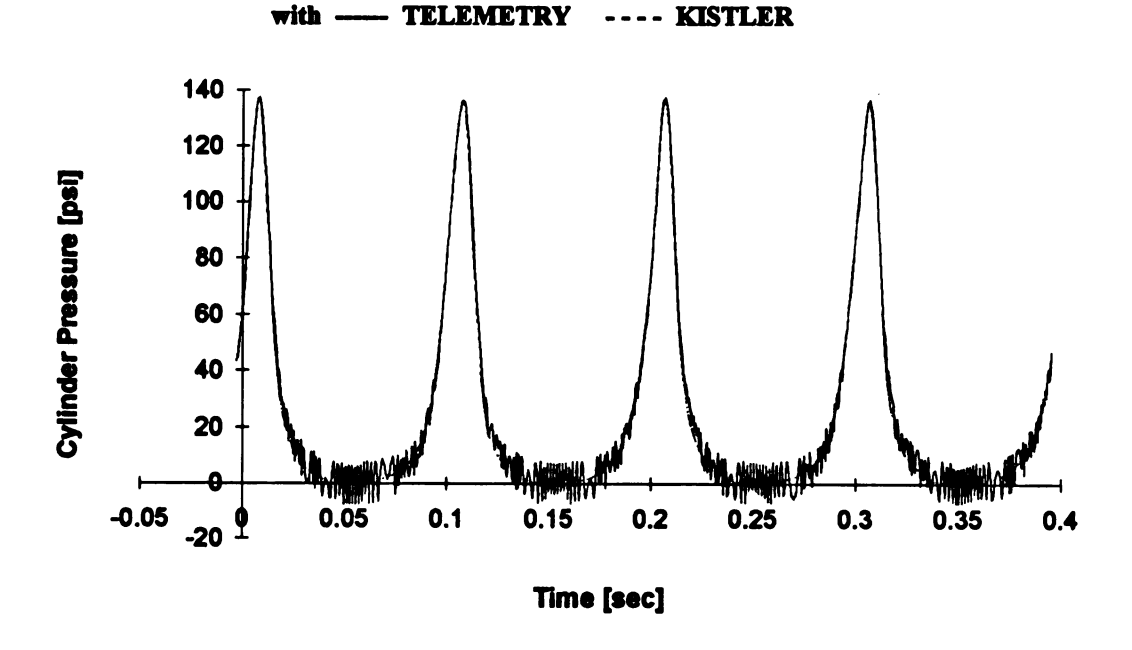


Figure 21: Compression Cycle at 604 rpm

---- KISTLER

with ---- TELEMETRY

Measured point No. 4 at 604 rpm (Figure 21) was considered bad data and the measuring was repeated (No. 5). Later the data was recovered and is shown in Figure 21.

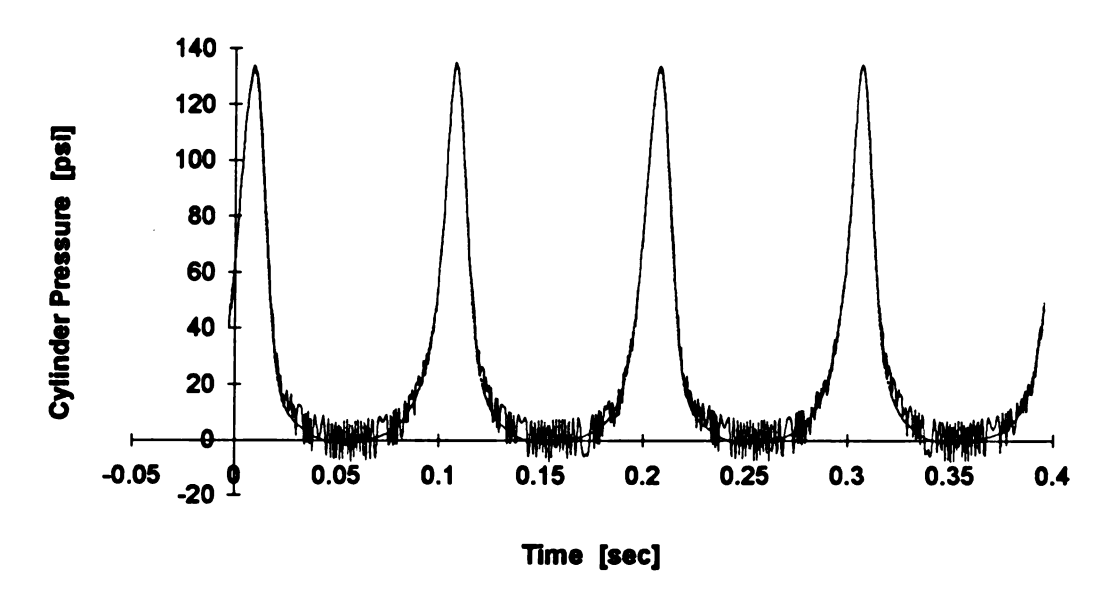


Figure 22: Compression Cycle at 598 rpm
with — TELEMETRY ---- KISTLER

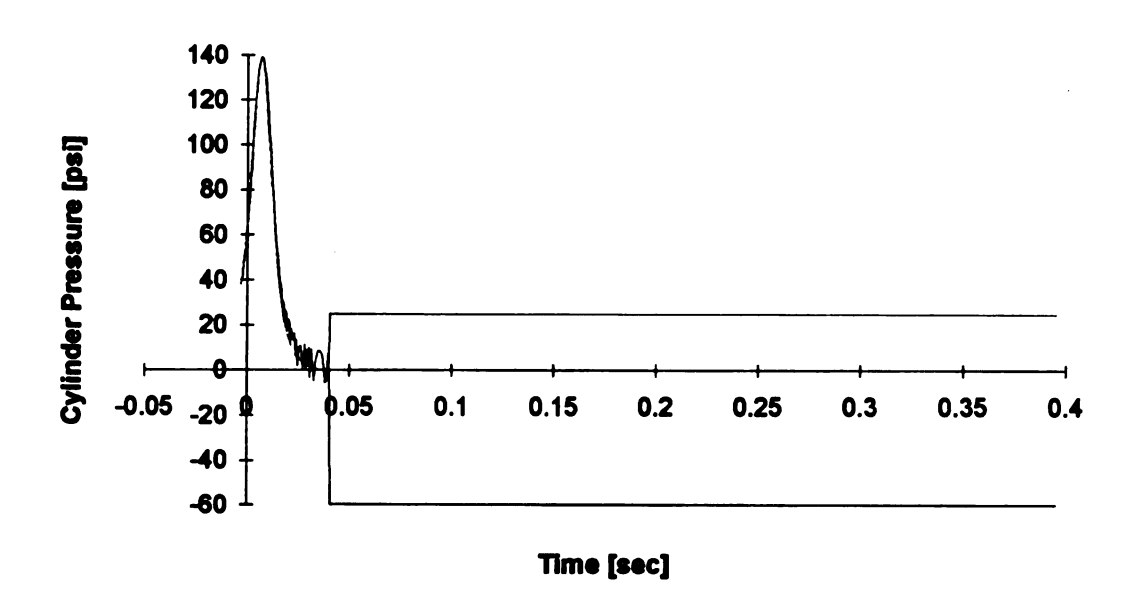


Figure 23: Compression Cycle at 711 rpm
with —— TELEMETRY ---- KISTLER

At 711 rpm the Nicolet Oscilloscope stored only the first msec data. After that all data points were set to zero. The two calibrated zeros are at -60 psi for the Kulite and at +25 psi for the Kistler quartz transducer. But it still can be seen that the two signals are superimposed (Figure 23).

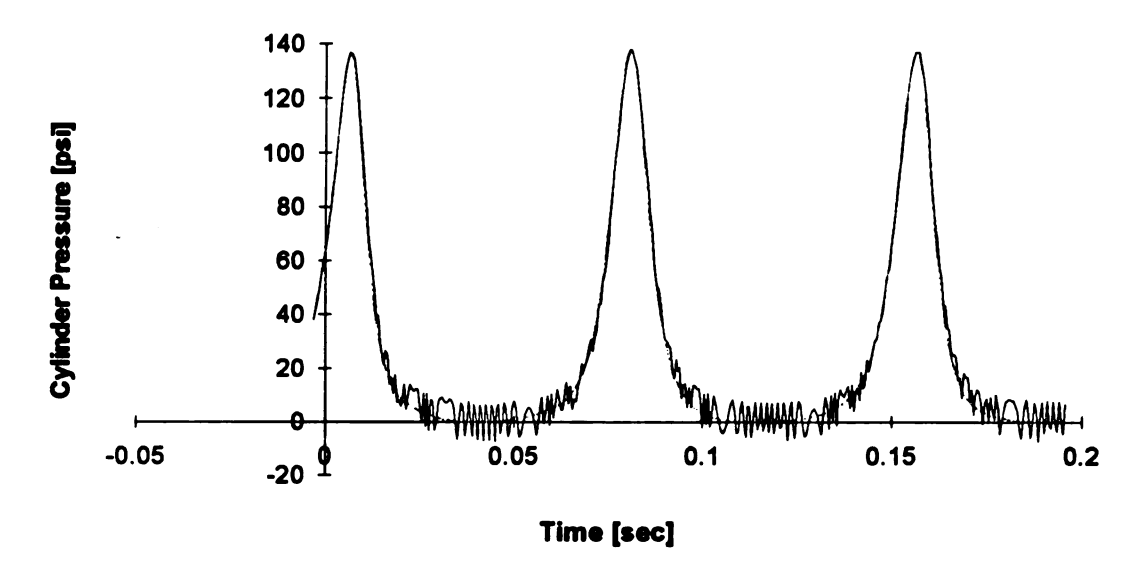


Figure 24: Compression Cycle at 801 rpm

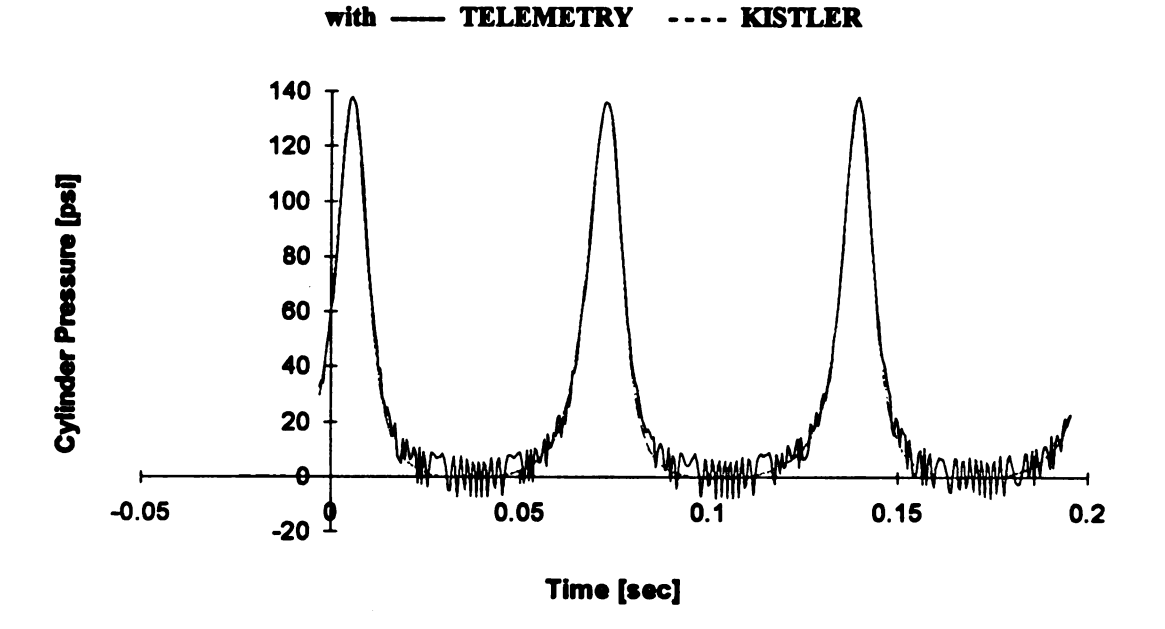


Figure 25: Compression Cycle at 899 rpm
with — TELEMETRY ---- KISTLER

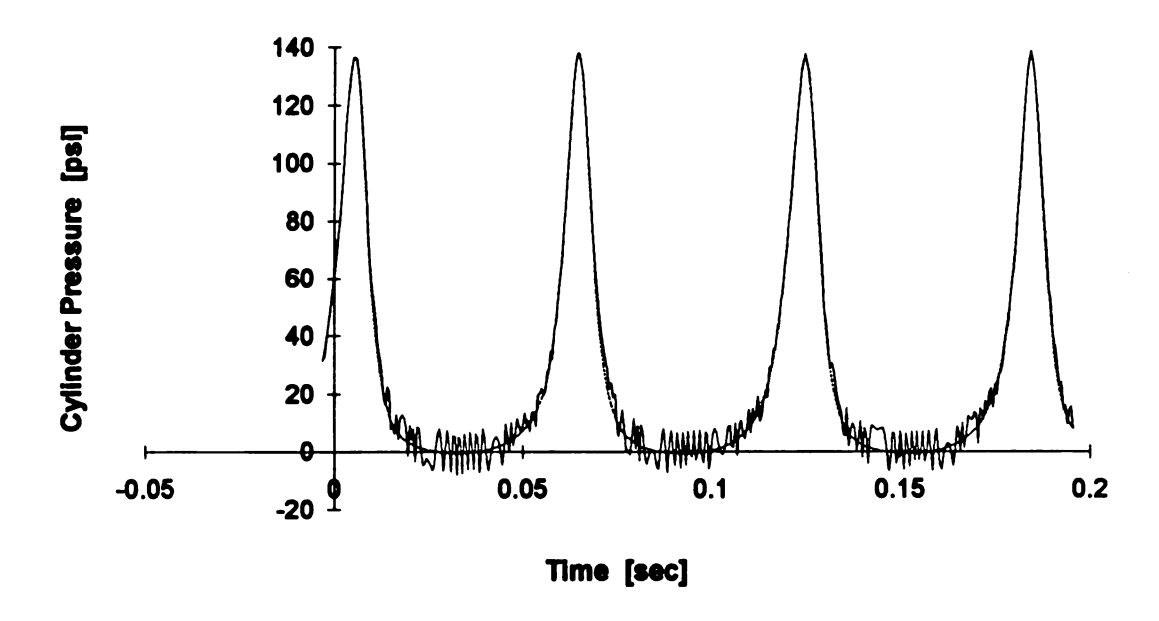


Figure 26: Compression Cycle at 1007 rpm
with —— TELEMETRY ---- KISTLER

After 1100 rpm (measured point 11, see table 2) the parts inside the cylinder reached a temperature equilibrium at about 100°C (200°F), which remained almost constant until the end of the test run. According to the KULITE pressure transducer datasheet, this causes the sensor to lose sensitivity of 1.5% per 100°F.

This sensitivity loss was numerically adjusted in EXCEL 4.0 for every speed above 1100 rpm. The calibration was changed to:

$$Pressure_{Kulite} = (Voltage_{after\ Telemetrv} - 0.54) \times 110.6 \times 1.03$$
 in psi

where 1.03 = 3 % temperature sensitivity loss compensation. The calibration for the Kistler quartz remained the same. But every measured point needed to be offset corrected before the Kistler quartz signal could be plotted and additional to that the Kistler charge amplifier was always reset before every data sampling. Again, this procedure is not necessary for the Kulite sensor.

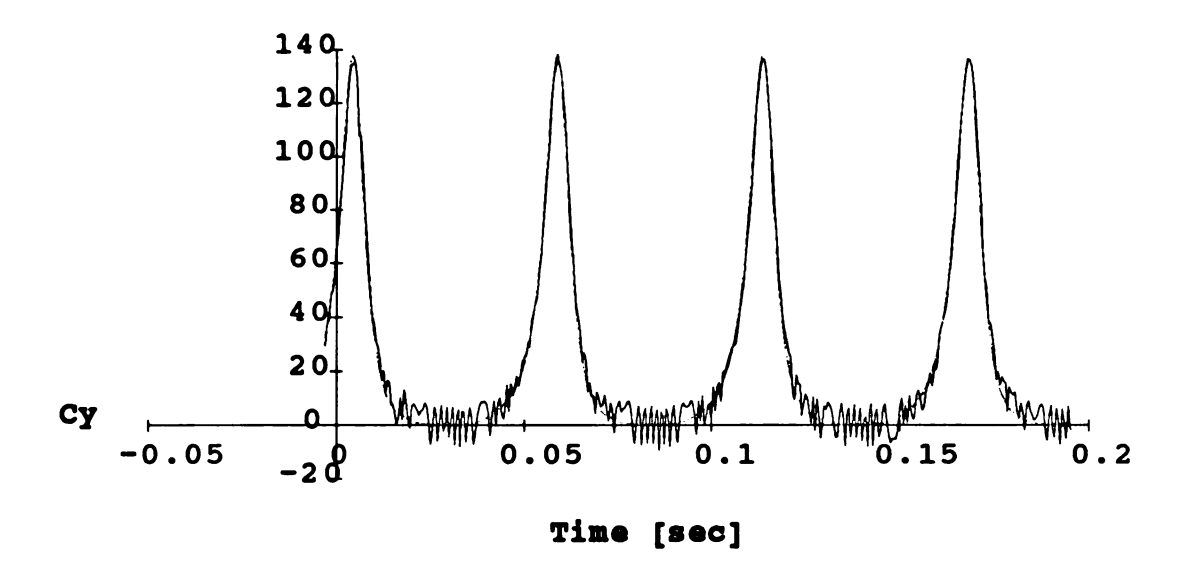


Figure 27: Compression Cycle at 1099 rpm
with —— TELEMETRY ---- KISTLER

At 1099 rpm the two signals are not superimposed anymore. A slight difference can be recognized at the maximum pressure. This is due to the temperature sensitivity loss of the Kulite transducer, a semi-conductor characteristic that all sensors with a silicon diaphragm have in common. The four resistors of the Wheatstone bridge, which are diffused into the silicon diaphragm loose more of their resistance the higher the temperature of the diaphragm gets.

33

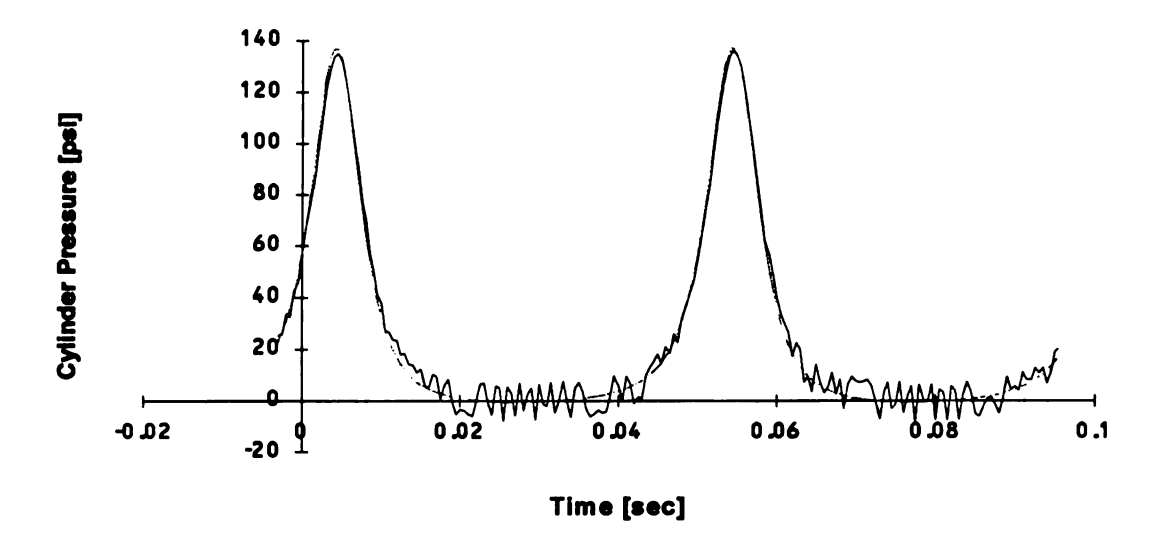


Figure 28: Compression Cycle at 1204 rpm

Telemetry Signal is Not Adjusted

with —— TELEMETRY ---- KISTLER

With the given temperature sensitivity drift of 3% at 200°F (see 4.2), the telemetry signal was adjusted in EXCEL 4.0 by multiplication.

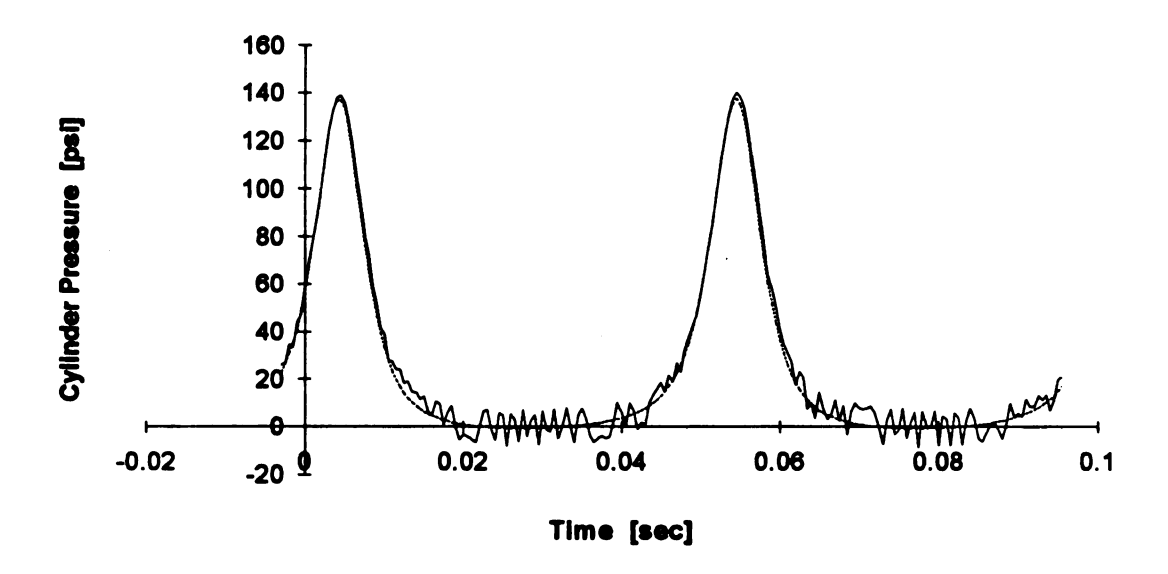


Figure 29: Compression Cycle at 1204 rpm

Telemetry Signal is Adjusted

with —— TELEMETRY ---- KISTLER

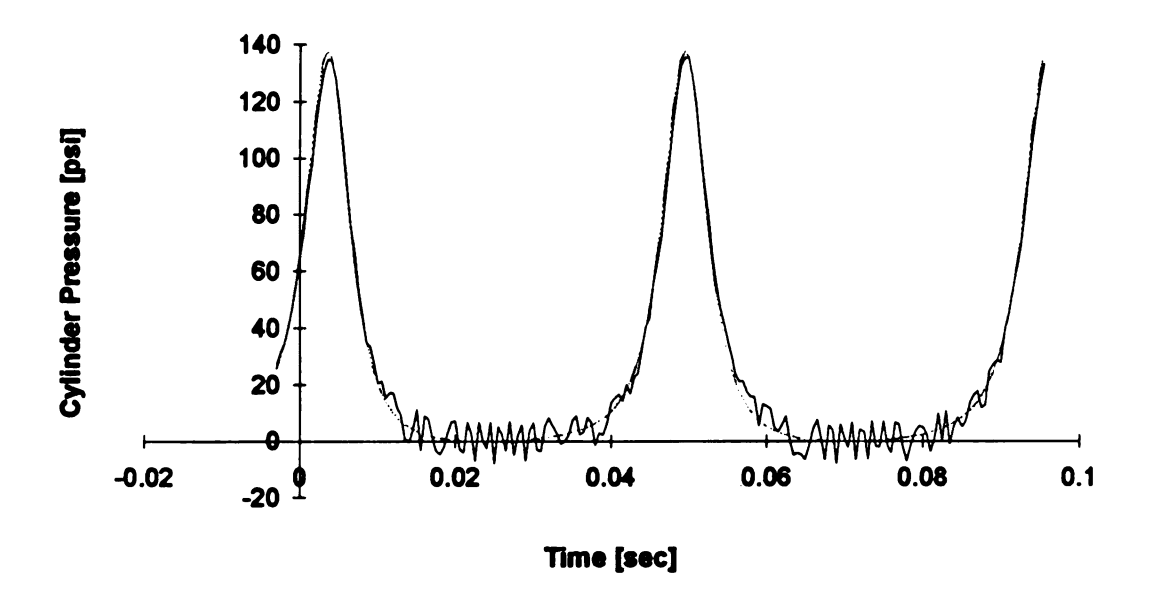


Figure 30: Compression Cycle at 1301 rpm

Telemetry Signal is Not Adjusted

with —— TELEMETRY ---- KISTLER

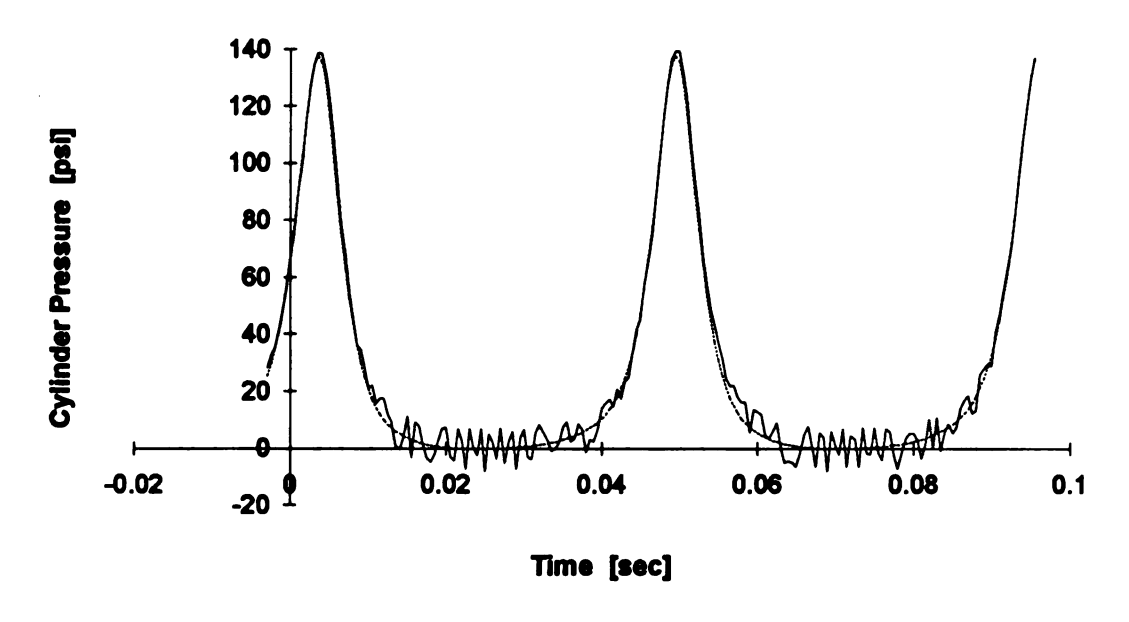


Figure 31: Compression Cycle at 1301 rpm

Telemetry Signal is Adjusted

with — TELEMETRY ---- KISTLER

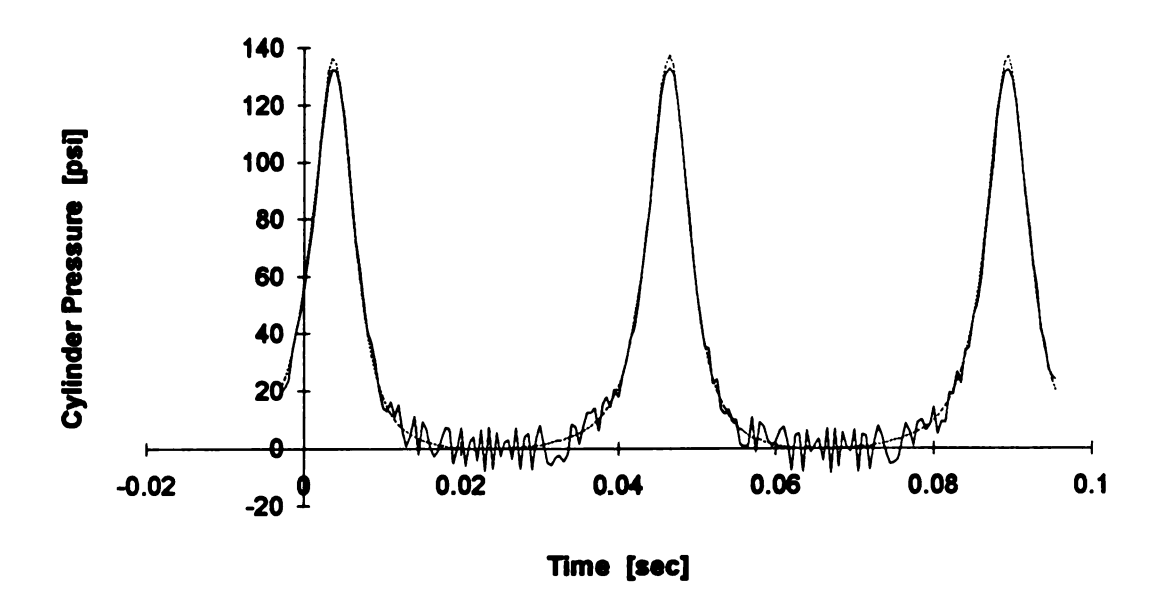


Figure 32: Compression Cycle at 1400 rpm

Telemetry Signal is Not Adjusted

with —— TELEMETRY ---- KISTLER

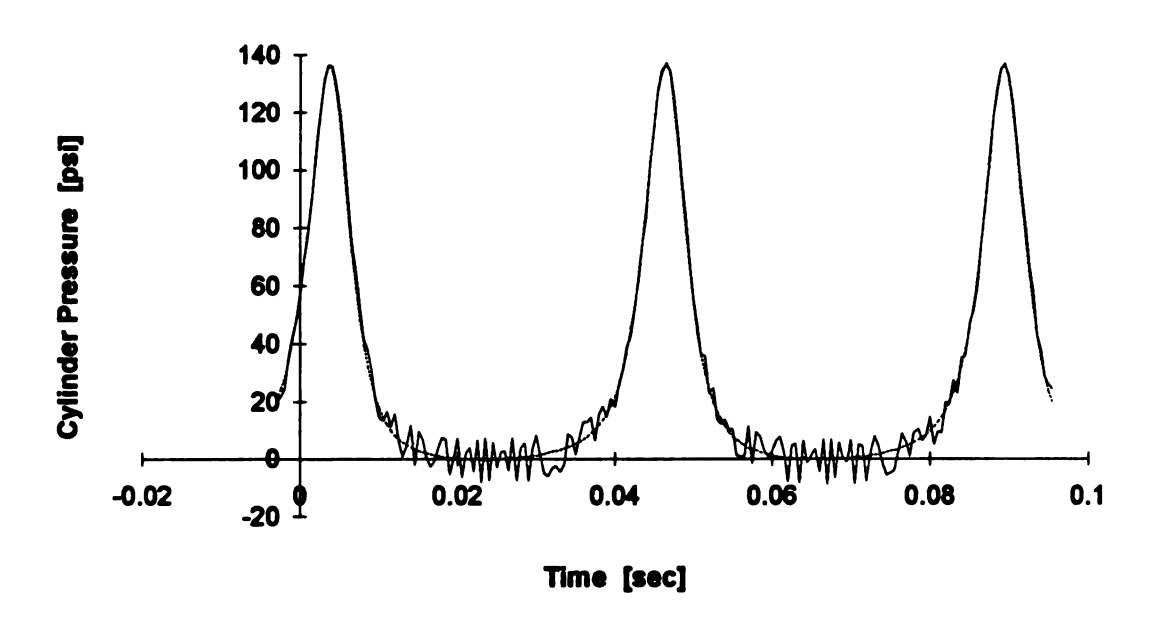


Figure 33: Compression Cycle at 1400 rpm

Telemetry Signal is Adjusted

with —— TELEMETRY ---- KISTLER

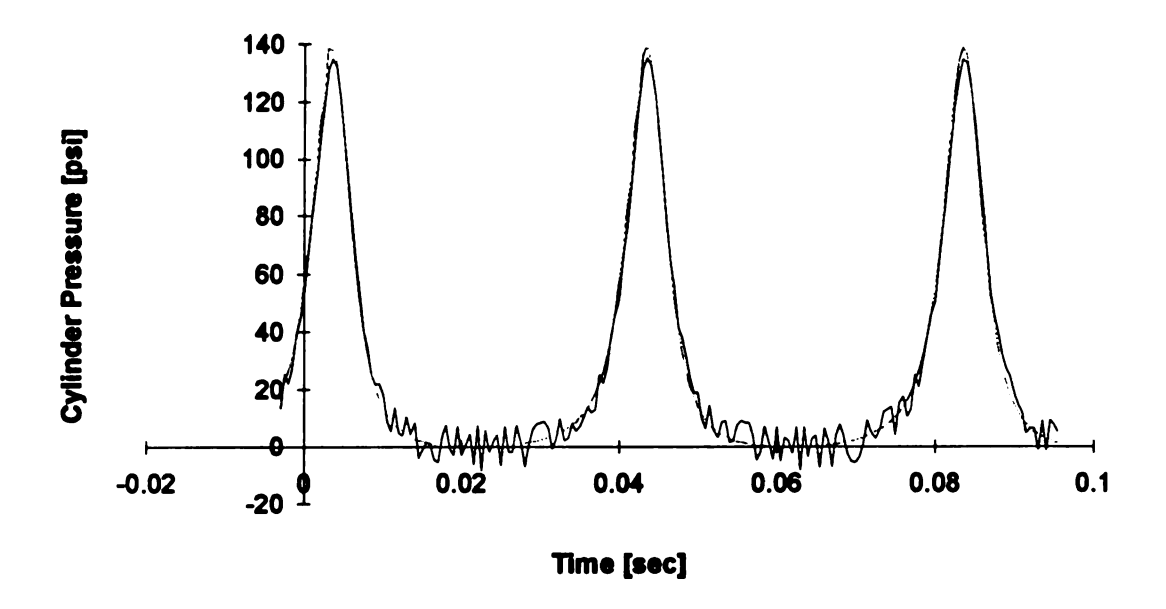


Figure 34: Compression Cycle at 1501 rpm

Telemetry Signal is Not Adjusted

with — TELEMETRY ---- KISTLER

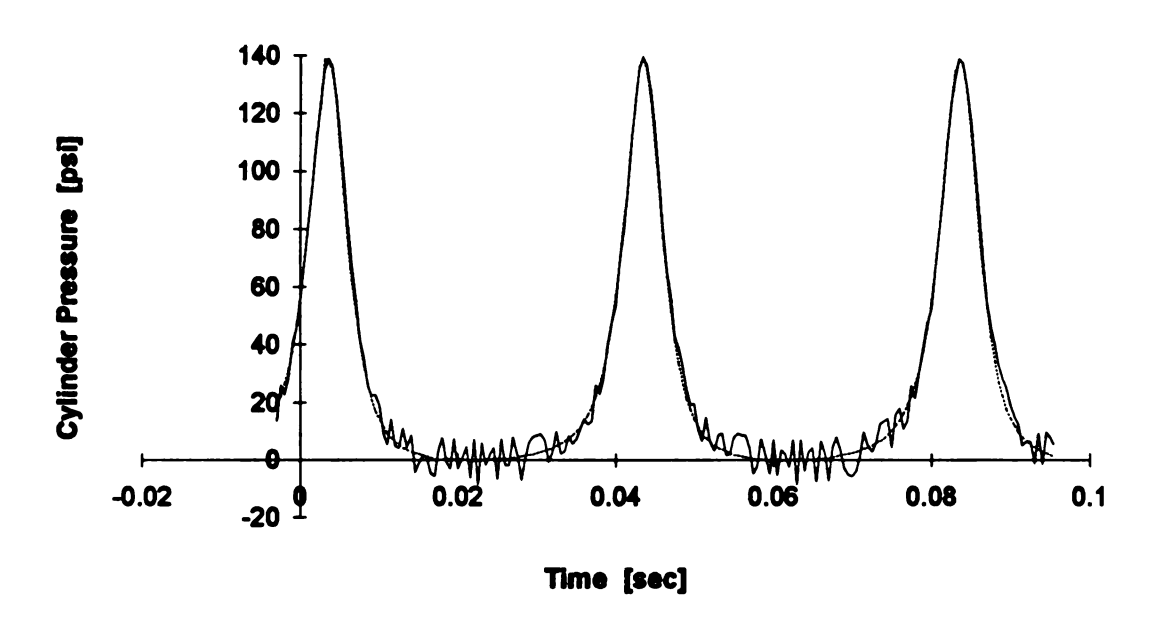


Figure 35: Compression Cycle at 1501 rpm

Telemetry Signal is Adjusted

with —— TELEMETRY ---- KISTLER

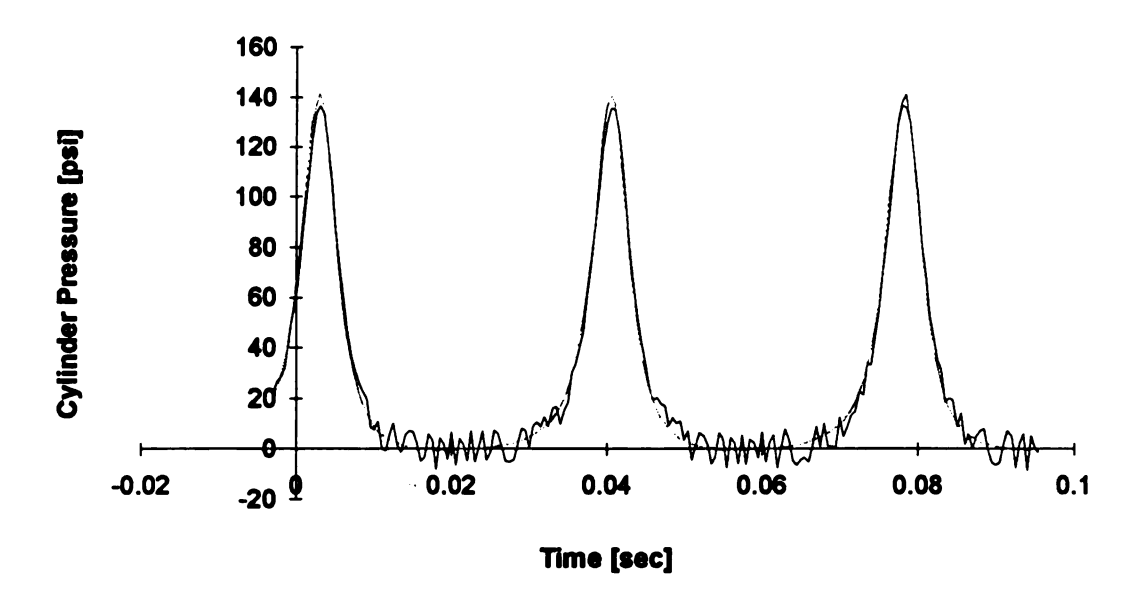


Figure 36: Compression Cycle at 1595 rpm

Telemetry Signal is Not Adjusted

with —— TELEMETRY ---- KISTLER

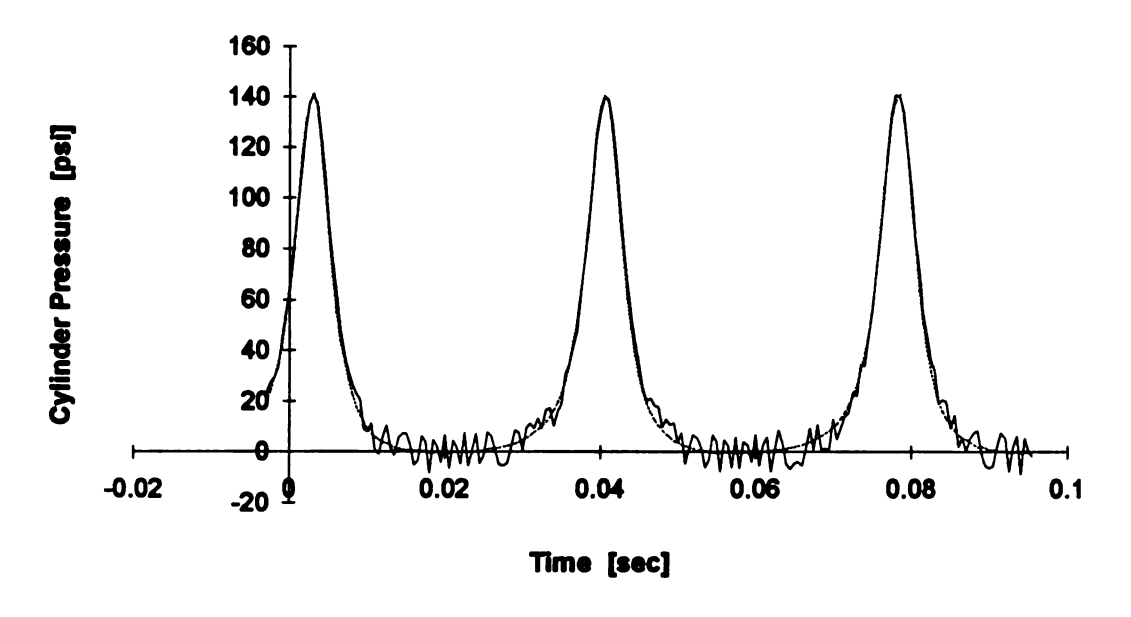


Figure 37: Compression Cycle at 1595 rpm

Telemetry Signal is Adjusted

with —— TELEMETRY ---- KISTLER

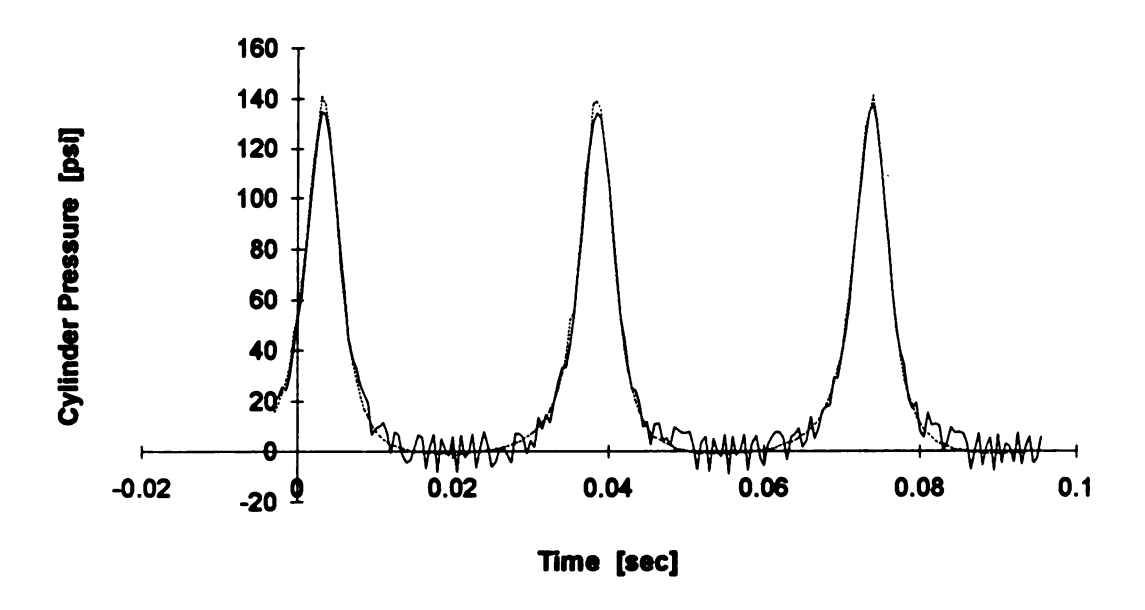


Figure 38: Compression Cycle at 1700 rpm

Telemetry Signal is Not Adjusted

with —— TELEMETRY ---- KISTLER

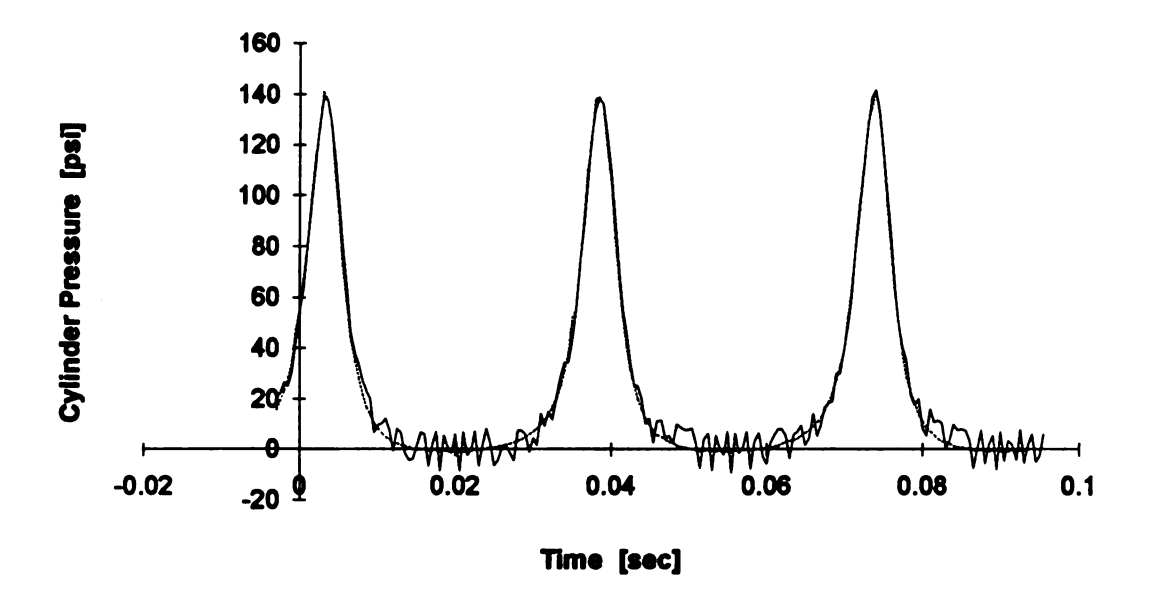


Figure 39: Compression Cycle at 1700 rpm

Telemetry Signal is Adjusted

with —— TELEMETRY ---- KISTLER

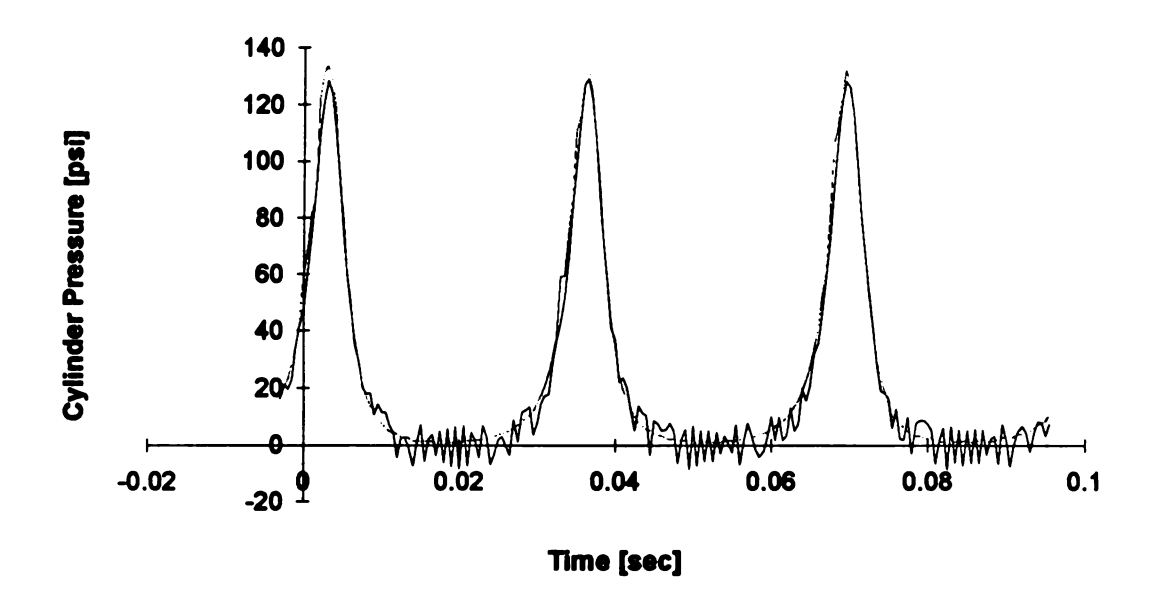


Figure 40: Compression Cycle at 1800 rpm

Telemetry Signal is Not Adjusted

with —— TELEMETRY ---- KISTLER

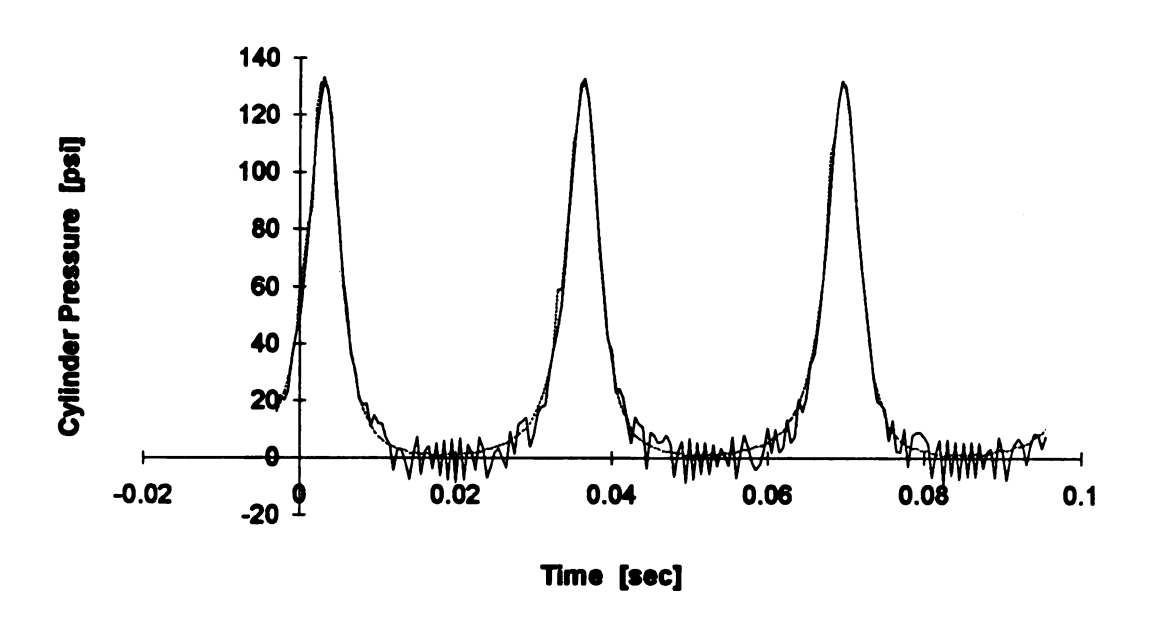


Figure 41: Compression Cycle at 1800 rpm

Telemetry Signal is Adjusted

with —— TELEMETRY ---- KISTLER

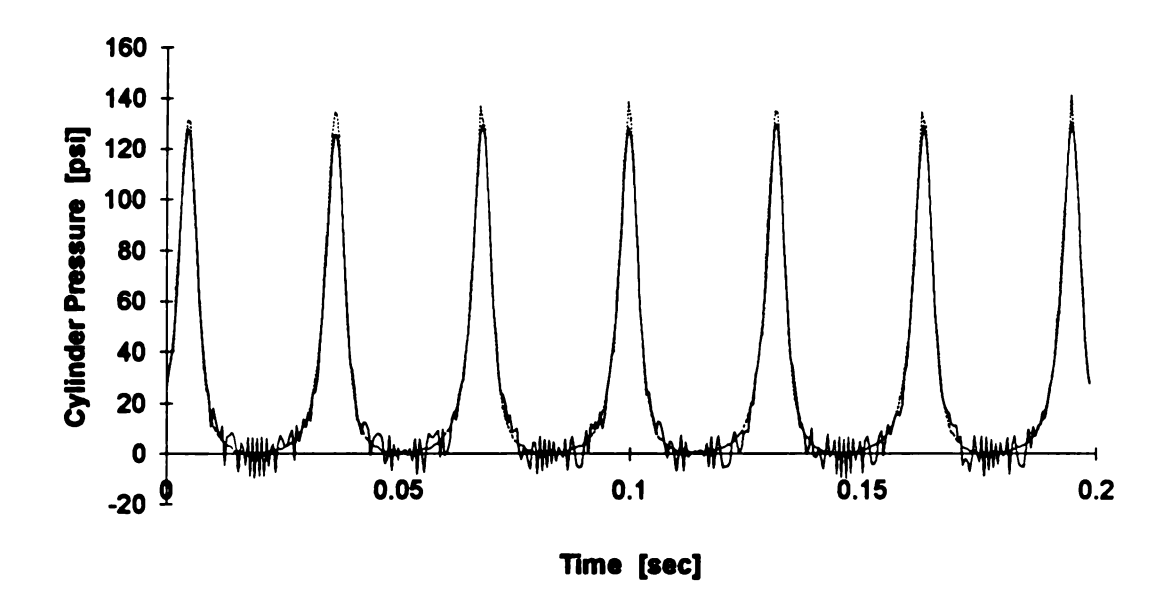


Figure 42: Compression Cycle at 1894 rpm

Telemetry Signal is Not Adjusted

with —— TELEMETRY ---- KISTLER

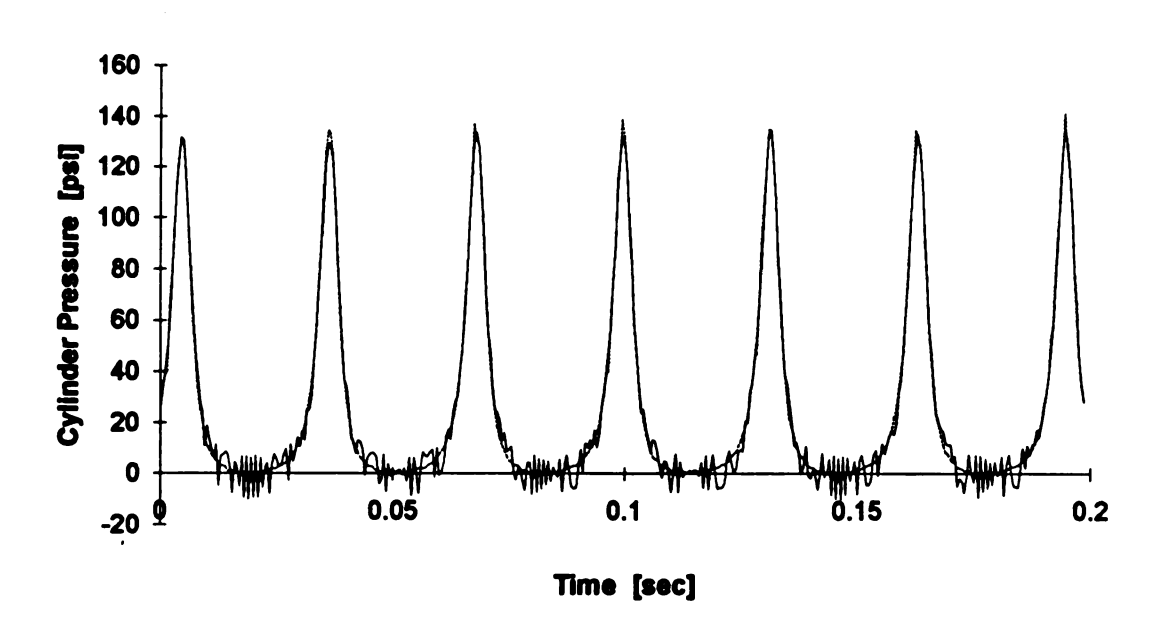


Figure 43: Compression Cycle at 1894 rpm

Telemetry Signal is Adjusted

with —— TELEMETRY ---- KISTLER

The highest speed where the prototype system delivered usable data was 2008 rpm.

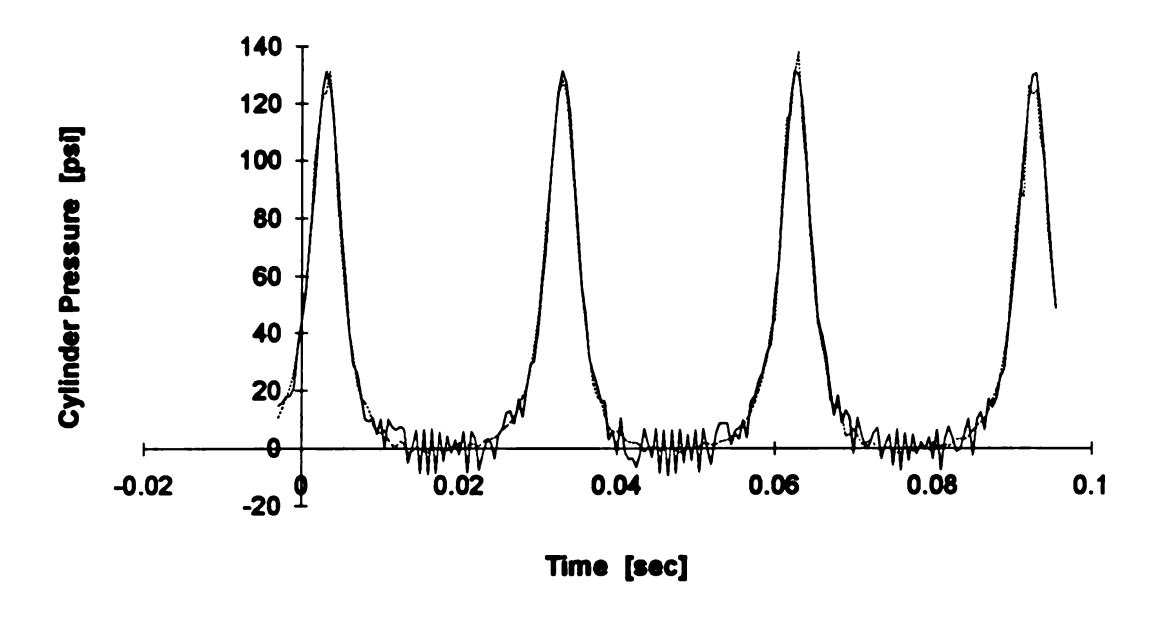


Figure 44: Compression Cycle at 2008 rpm

Telemetry Signal is Adjusted

with —— TELEMETRY ---- KISTLER

All of the test data was digitized at the same sample rate. The signals of higher speeds are represented with fewer datapoints per revolution and do not look as smooth as those sampled at lower speeds. This might become more noticeable at speeds higher than 2000 rpm.

At 2095 rpm the telemetry signal broke down every revolution. As Figure 45 shows the telemetry follows the cylinder pressure up to 120 psi to drop down suddenly to -60 psi (which equals a zero volt signal). This can be caused by either a cold soldered joint (always possible in prototypes) or the damaged power supply cable (see Figures 17, 45, 46).

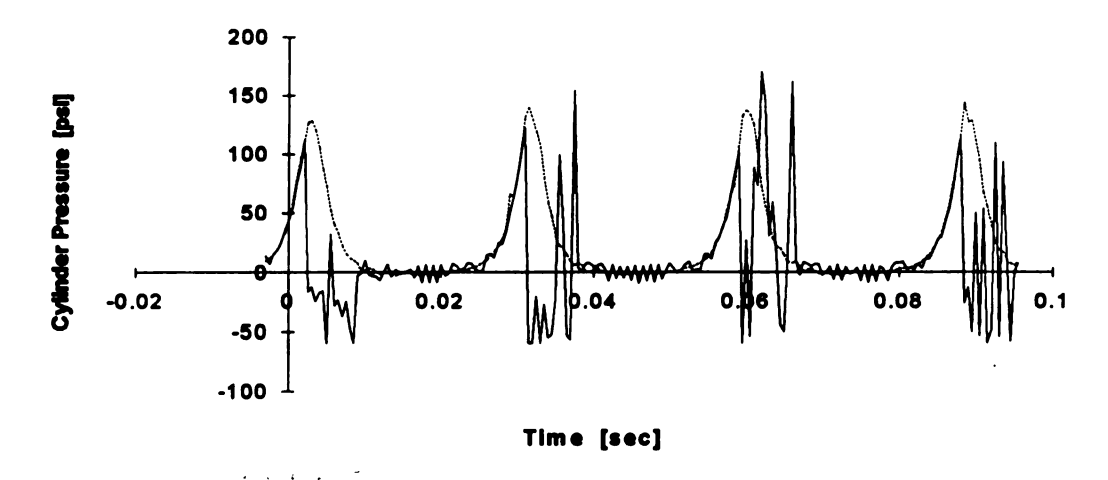


Figure 45: Compression Cycle at 2095 rpm

Failure in Telemetry Power Supply

with —— TELEMETRY ---- KISTLER

This failure also happened at the highest test speed, at 2250 rpm. The telemetry signal followed the pressure only up to 80 psi (120 psi at 2095 rpm). This suggests an acceleration-caused failure, like a cold solder joint or a strongly vibrating power supply cable (Figure 46).

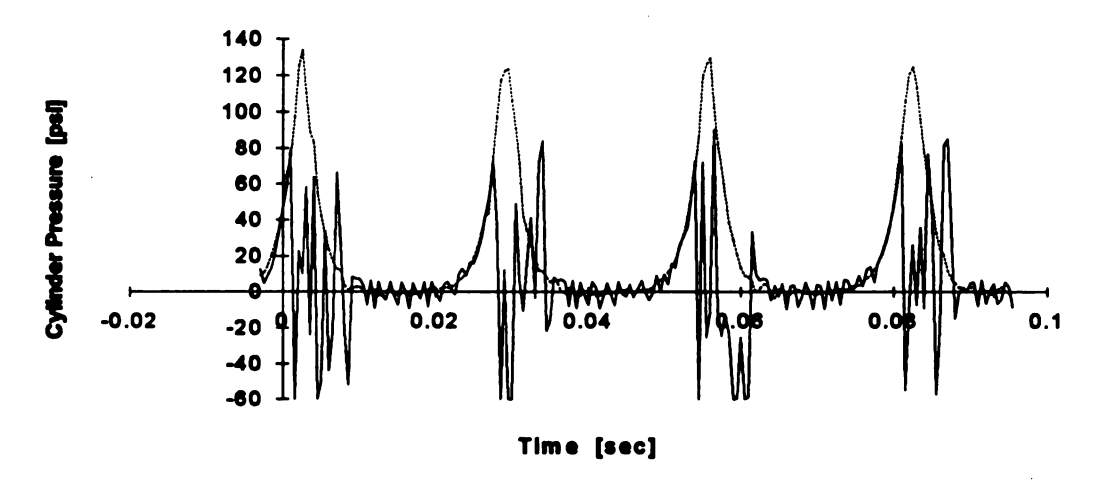


Figure 46: Compression Cycle at 2250 rpm

Failure in Telemetry Power Supply

with —— TELEMETRY ---- KISTLER

6.0 SUMMARY AND CONCLUSIONS

In this project an infrared telemetry was designed, tested and its feasibility proved for the interior of a piston engine. To use this technology in a firing engine configuration several changes will have to be made:

- The sender circuit board has to be built in surface mount technology. This will avoid cold solder joints and will increase the stability of the whole circuit board.
- The frequency output for low transducer voltage output should be increased to eliminate the noise at low pressures.
- The DC power supply of the sender board has to be improved. A "grasshopper" linkage between crank case and piston will yield a constant DC voltage supply. An additional capacitor within the piston will help stabilizing this voltage.
- The pressure transducer has to be changed from the XCQ 093 to the high temperature and pressure model XCE 093. Both transducers have the same dimensions.

The results of the present study can be summarized as follows:

1. The investigated telemetry system is a suitable data transmission system for a piston engine.

- 2. There are no limitations in the type of sensors that can be used as long as they have a voltage output. Thermocouples, pressure transducers and displacement sensors are suitable to the telemetry system, because the range of transmitted voltage is adjustable across a wide range.
- 3. The designed system is expandable to a multiple channel system, which can be used for example to compensate the temperature drift of a pressure transducer.
- 4. This telemetry makes, for the first time ever, certain processes in a combustion engine accessible for research such as piston ring movements over a long time period, pressure decreases along different kinds of piston rings, blow-by between cylinder wall and piston, piston temperatures and others.



APPENDIX

Piston Acceleration

The piston acceleration is a very important parameter in a piston engine [5, 7, 8, 9]. It can be derived from the piston displacement (Figure 47).

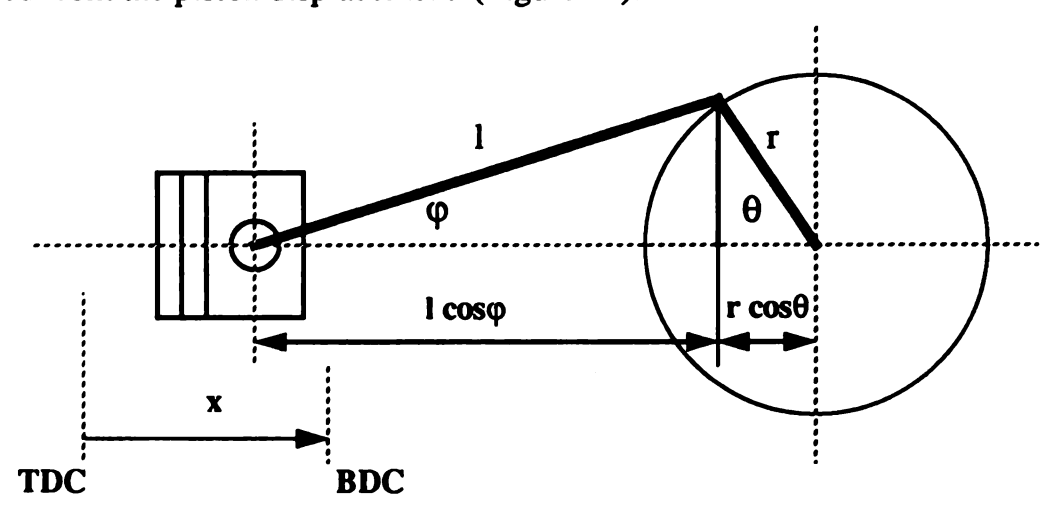


Figure 47: Piston Displacement x

From the above picture two equations can be derived:

(1)
$$l\sin\varphi = r\sin\theta$$
 and $\lambda = \frac{r}{l}$ yield an expression for φ : $\sin\varphi = \lambda\sin\theta$

(2) The piston displacement can be written as $x = l(1-\cos\phi) + r(1-\cos\theta)$, where $\cos\phi$ can be replaced with $\cos\phi = \sqrt{1 - \lambda^2 \sin^2\theta} \qquad \text{from } \sin\phi = \lambda \sin\theta \qquad (1) \quad \text{to}$

$$x = r \left[1 - \cos\theta + \frac{1 - \sqrt{1 - \lambda^2 \sin^2\theta}}{\lambda} \right]$$
 (2)

The second derivate of this function gives the piston acceleration, but it is easier to use the Taylor series [10]

$$(1+z)^{\kappa} = 1 + \kappa z + \frac{\kappa(\kappa-1)}{2!} z^2 + \frac{\kappa(\kappa-1)(\kappa-2)}{3!} z^3 + \dots$$
 for $|z| < 1$

which is

$$\sqrt{1-z} = 1 - \frac{1}{2}z - \frac{1}{8}z^2 - \frac{1}{16}z^3 - \frac{5}{128}z^4 + \dots \qquad \text{with} \qquad z = -\sqrt{\lambda^2 \sin^2 \theta}$$

SO

$$x = r \left[1 - \cos\theta + \frac{\lambda}{2}\sin^2\theta + \frac{\lambda^3}{8}\sin^4\theta + \frac{\lambda^5}{16}\sin^6\theta + \frac{5\lambda^7}{128}\sin^8\theta \dots \right]$$

with this the maximum error can be calculated at $\theta = 90^{\circ}$:

$$x = r \left[1 - \cos \theta + \frac{\lambda}{2} \sin^2 \theta \right]$$
 0.3475% error

$$x = r \left[1 - \cos\theta + \frac{\lambda}{2}\sin^2\theta + \frac{\lambda^3}{8}\sin^4\theta \right]$$
 0.0175% error

$$x = r \left[1 - \cos\theta + \frac{\lambda}{2}\sin^2\theta + \frac{\lambda^3}{8}\sin^4\theta + \frac{\lambda^5}{16}\sin^6\theta \right]$$
 0.00106% error

$$x = r \left[1 - \cos\theta + \frac{\lambda}{2}\sin^2\theta + \frac{\lambda^3}{8}\sin^4\theta + \frac{\lambda^5}{16}\sin^6\theta + \frac{5\lambda^7}{128}\sin^8\theta \right]$$
 0.00007% error

so with
$$x = r \left[1 - \cos \theta + \frac{\lambda}{2} \sin^2 \theta + \frac{\lambda^3}{8} \sin^4 \theta \right]$$

the error is reasonably low.

This fuction will be used for further calcuations.

With

$$\sin^2\theta = \frac{1}{2} - \frac{1}{2}\cos 2\theta$$

$$\sin^4 \theta = \frac{3}{8} - \frac{1}{2}\cos 2\theta + \frac{1}{8}\cos 4\theta$$
 from [11]

the piston displacement can be rewritten

$$x = r \left[1 - \cos\theta + \frac{\lambda}{4} \left(1 + \frac{3\lambda^2}{16} - \left(1 + \frac{\lambda^2}{4} \right) \cos 2\theta + \left(\frac{\lambda^2}{16} \right) \cos 4\theta \right) \right]$$

$$v = \frac{dx}{dt} = r\omega \left[\sin\theta + \frac{\lambda}{2} \left[(1 + \frac{\lambda^2}{4}) \sin 2\theta - \frac{\lambda^2}{8} \sin 4\theta \right] \right]$$
 with $\theta = \omega t$

the piston acceleration is

$$a = \frac{d^2x}{dt^2} = r\omega^2 \left[\cos\theta + \lambda \left[(1 + \frac{\lambda^2}{4}) \cos 2\theta - \frac{\lambda^2}{4} \cos 4\theta \right] \right]$$

to check the remaining error of this function equation (1) has to be differentiated twice to get on the exact solution of the piston acceleration:

$$x = r \left[1 - \cos\theta + \frac{1 - \sqrt{1 - \lambda^2 \sin^2\theta}}{\lambda} \right]$$

$$v = \dot{x} = r\omega \left[\sin\theta + \frac{\lambda^2 2 \sin\theta \cos\theta}{2\lambda\sqrt{1 - \lambda^2 \sin^2\theta}} \right] = r\omega \left[\sin\theta + \frac{\lambda \sin2\theta}{2\sqrt{1 - \lambda^2 \sin^2\theta}} \right]$$
Term I II

Term II is far more difficult to derive. Its differentiation is shown below:

with
$$dv/dt = v'u + u'v$$
 and $u = \frac{\lambda}{2}\sin 2\theta$ and $v = (1 - \lambda^2 \sin^2 \theta)^{-1/2}$
and $\frac{d\sin^2 \theta}{dt} = \frac{d(\sin \theta \sin \theta)}{dt} = \sin \theta \cos \theta + \cos \theta \sin \theta = \sin 2\theta$

$$\frac{d(TermII)}{dt} = \frac{\lambda}{2} \frac{2\cos 2\theta}{\sqrt{1 - \lambda^2 \sin^2 \theta}} + \frac{\lambda}{2} \sin 2\theta \left(-\frac{1}{2}\right) \frac{-\lambda^2 \sin 2\theta}{\sqrt{\left(1 - \lambda^2 \sin^2 \theta\right)^3}}$$

now Term II is brought on a common denominator:

$$\frac{d(TermII)}{dt} = \lambda \frac{(1 - \lambda^2 \sin^2 \theta) \cos 2\theta + \frac{\lambda^2}{4} \sin^2 2\theta}{\sqrt{(1 - \lambda^2 \sin^2 \theta)^3}} =$$

$$= \lambda \frac{\cos 2\theta - \lambda^2 \sin^2 \theta \cos 2\theta + \frac{\lambda^2}{4} \sin^2 2\theta}{\sqrt{(1 - \lambda^2 \sin^2 \theta)^3}}$$

with two function-product relations from [12]

$$\sin\alpha\sin\beta\cos\gamma = \frac{1}{4}\left[-\cos\left(\alpha+\beta-\gamma\right) + \cos\left(\beta+\gamma-\alpha\right) + \cos\left(\gamma+\alpha-\beta\right) + \\ + \cos\left(\alpha+\beta+\gamma\right)\right] = \sin^2\theta\cos\theta = \frac{1}{4}\left[2\cos2\theta - \cos4\theta - 1\right]$$
$$\sin^2\alpha = \frac{1}{2}\left[1 - \cos2\theta\right] = \sin^22\theta = \frac{1}{2}\left[1 - \cos4\theta\right]$$

the derivative of term II is

$$\frac{d\left(TermII\right)}{dt} = \lambda \frac{\cos 2\theta - \frac{\lambda^2}{2}\cos 2\theta + \frac{\lambda^2}{4}\cos 4\theta + \frac{\lambda^2}{4} + \frac{\lambda^2}{8} - \frac{\lambda^2}{8}\cos 4\theta}{\sqrt{\left(1 - \lambda^2 \sin^2\theta\right)^3}}$$

With the expression from [12]

$$\sin^4\alpha = \frac{1}{8} \left[\cos 4\alpha - 4\cos 2\alpha + 3 \right]$$

the exact acceleration of the reciprocating piston can be written as

$$a = \frac{dv}{dt} = \ddot{x} = r\omega^{2} \left[\cos\theta + \lambda \frac{\cos 2\theta + \lambda^{2} \sin^{4}\theta}{\sqrt{(1 - \lambda^{2} \sin^{2}\theta)^{3}}} \right]$$

Finally with the exact solution

$$a = \frac{dv}{dt} = \ddot{x} = r\omega^{2} \left[\cos\theta + \lambda \frac{\cos 2\theta + \lambda^{2} \sin^{4}\theta}{\sqrt{(1 - \lambda^{2} \sin^{2}\theta)^{3}}} \right]$$

the remaining error of the Taylor series approximation can be calculated

$$a = \frac{d^2x}{dt^2} = r\omega^2 \left[\cos\theta + \lambda \left[(1 + \frac{\lambda^2}{4})\cos 2\theta - \frac{\lambda^2}{4}\cos 4\theta \right] \right]$$

The errors are for (at $\theta = 90^{\circ}$)

$$a = \frac{d^2x}{dr^2} = r\omega^2 \left[\cos\theta + \lambda \left[\left(1 + \frac{\lambda^2}{4}\right)\cos 2\theta \right] \right]$$
 2.7 %

$$a = \frac{d^2x}{dt^2} = r\omega^2 \left[\cos\theta + \lambda \left[(1 + \frac{\lambda^2}{4}) \cos 2\theta - \frac{\lambda^2}{4} \cos 4\theta \right] \right]$$
 0.37 %

For the maximum acceleration (at $\theta = 0^{\circ}$ and $\theta = 180^{\circ}$) we find with the exact solution:

$$a_{TDC} = r\omega^2(\cos\theta + \lambda\cos 2\theta) = r\omega^2(1+\lambda)$$
 at $\theta = 0^{\circ}$ (TDC)

$$a_{BDC} = r\omega^2(\cos\theta + \lambda\cos 2\theta) = -r\omega^2(1-\lambda)$$
 at $\theta = 180^{\circ}$ (BDC)

The remaining errors for the Taylor series approximation are

$$a_{TDC} = \frac{d^2x}{dt^2} = r\omega^2 \left[\cos\theta + \lambda \left[(1 + \frac{\lambda^2}{4}) \cos 2\theta \right] \right]$$
0.58 %

$$a_{TDC} = \frac{d^2x}{dt^2} = r\omega^2 \left[\cos\theta + \lambda \left[(1 + \frac{\lambda^2}{4})\cos 2\theta - \frac{\lambda^2}{4}\cos 4\theta \right] \right] \qquad 0.00046 \%$$



LIST OF REFERENCES

- 1. Fujimoto, H., Yoshihara, Y., Goto, T., Furahama, S., "Measurement of Cylinder Bore Deformation During Actual Operating Engines", Musashi Institute of Technology and Nissan Motor Corporation, SAE Paper 910042, 1990.
- "Kolbenringbewegungsmessung an der neuen Baureihe 595", 1991 1992,
 Meβbericht der MTU Friedrichshafen, Deutschland, 1992.
- 3. Barna, Glen, "Piston Temperature Measurements", IR Telemetry Instrument Datasheet, IR telemetrics, Houghton, MI, 1991.
- 4. Schock, H., Sober, S., "Measurement and Analysis of Dynamic Piston Ring Pack Pressures", Proposal Michigan State University, 1992.
- 5. Taylor, C. F., "The Internal Combustion Engine in Theory and Praxis", MIT Press, 1985 (Volume 2).
- 6. Beitz, Küttner, "Dubbel, Taschenbuch für den Maschinenbau", 14. Auflage, Springer, 1981.
- 7. Heywood, J. B., "Internal Combustion Engine Fundamentals", McGraw-Hill, 1988.

- 8. Abramowitz, M., Stegun, I. A., "Handbook of Mathematical Functions", Dover, 1972.
- 9. Pischinger, F., "Verbrennungsmotoren", RWTH Aachen, Deutschland, 1987, (Volume 1).
- 10. Groh, K., "Grundzüge des Kolbenmaschinenbaus", Universität Hannover, Deutschland, 1975 (Volume 1).
- 11. Beyer, W. H., "CRC Standard Mathematical Tables", CRC Press, 1978.
- 12. Bartsch, H. J., "Mathematische Formeln", VEB Fachbuchverlag Leipzig, DDR, 1988.
- 13. Van Wylen, G. J., Sonntag, R. E., "Fundamentals of Classical Thermodynamics", 3rd Edition, Wiley, 1986.